

1-1-2012

Measuring the Effects of Temperature on Optical Propagation in Heated Tissues Using Point Radiance Spectroscopy

Radoslaw Sadowski
Ryerson University

Follow this and additional works at: <http://digitalcommons.ryerson.ca/dissertations>

 Part of the [Bioimaging and biomedical optics Commons](#), [Medical Biophysics Commons](#), and the [Optics Commons](#)

Recommended Citation

Sadowski, Radoslaw, "Measuring the Effects of Temperature on Optical Propagation in Heated Tissues Using Point Radiance Spectroscopy" (2012). *Theses and dissertations*. Paper 801.

**Measuring the Effects of Temperature on Optical Propagation in Heated
Tissues Using Point Radiance Spectroscopy**

By

Radoslaw Sadowski

B.Eng., Ryerson University, 2009

A thesis

presented in partial fulfillment

of the requirement for the degree of

Master of Science

in the Program of

Biomedical Physics

Toronto, Ontario, Canada, 2012

© Radoslaw Sadowski, 2012

Author's Declaration

I hereby declare that I am the sole author of this thesis. This is a true copy of the thesis, including any required final revisions, as accepted by my examiners.

I authorize Ryerson University to lend this thesis to other institutions or individuals for the purpose of scholarly research.

I further authorize Ryerson University to reproduce this thesis by photocopying or by other means, in total or in part, at the request of other institutions or individuals for the purpose of scholarly research.

I understand that my thesis may be made electronically available to the public.

Measuring the Effects of Temperature on Optical Propagation in Heated Tissues Using Point Radiance Spectroscopy

Radoslaw Sadowski, M.Sc., Biomedical Physics, Ryerson University, Toronto, 2012

Abstract

Laser interstitial thermal therapy (LITT) is a minimally invasive therapy in which light is delivered using optical fibers inserted into tissue to treat malignant tumours. Heating tissue above 55°C causes tissue coagulation, creating non-viable tissue. Previous work has demonstrated that radiance measurements are sensitive to heat-induced changes in tissue optical properties. This study investigates the use of radiance measurements to differentiate permanent temperature-induced changes in optical propagation, which reflect thermal damage, from any transient changes in optical propagation.

Experiments in water using our white-light point radiance spectroscopy (PRS) technique demonstrate that PRS is sensitive to detect optical absorption and temperature-dependence in the optical absorption of water, and a change in the acceptance cone with temperature. Experimental results using PRS in heated *ex vivo* porcine tissue show that the optical signal mainly represents permanent thermal damage and only a small part of the signal represent a temperature-dependent change due to water.

Acknowledgments

I would like to thank my supervisors Dr. Carl Kumaradas, Dr. Robert Weersink and Dr. William Whelan for all their help and guidance throughout my graduate studies and giving me the opportunity to work with them. Also, I would like to thank my committee member Dr. Michael Kolios. Thank you all for your questions, discussions and advising me throughout my studies.

In addition, I would like to thank Arthur Worthington at Ryerson University as well as Dr. Serge Grabtchack and Tyler Palmer at UPEI for helping me with my experimental set-up. I would also like to thank all the group members both at Ryerson and UPEI for creating a positive work environment.

Special thanks to my family and friends for their support throughout my studies. I would also like to thank all the graduate students, staff and faculty members in the Department of Physics at Ryerson University for making this a fun experience.

Table of Contents

Author's Declaration.....	ii
Abstract.....	iii
Acknowledgments.....	iv
Table of Contents.....	v
List of Figures.....	vii
List of Tables.....	xi
1 Introduction.....	1
1.1 Conventional Cancer Treatments.....	1
1.2 Thermal Therapy.....	1
1.3 Real-Time Monitoring of LITT.....	4
1.4 Optical Monitoring of LITT.....	5
1.5 Project Overview.....	8
2 Theory.....	10
2.1 Optical Properties of Tissue.....	10
2.2 Index of Refraction.....	13
2.3 Radiative Transport.....	15
3 Materials and Methods.....	17
3.1 Experiment #1: Measurements in Water.....	17
3.2 Experiment #2: Measurements in <i>Ex Vivo</i> Tissue.....	22
3.3 Theoretical Radiance Calculations.....	28
3.4 Data Analysis.....	31
4 Results and Discussion.....	32
4.1 Experiment #1: Water.....	32
4.1.1 Detecting Optical Absorption of Water.....	32
4.1.2 Temperature-Dependent Changes in Water Absorption.....	34
4.1.3 Temperature-Dependent Changes in the Acceptance Angle.....	36

4.2	Experiment #2: <i>Ex Vivo</i> Tissue	40
4.2.1	Dynamic Change in the Radiance Signal with Heating.....	40
4.2.2	Comparing the Radiance of Heated Tissue with Cooled Tissue.....	44
	Theoretical Radiance Results.....	52
5	Conclusion and Future Work	55
5.1	Conclusions	55
5.2	Future Work	56
	Appendix.....	58
A	Additional Measurements in <i>Ex Vivo</i> Tissue	58
B	Diffuse Reflectance Measurements	67
	Bibliography	71

List of Figures

Figure 1.2.1: Gross picture of canine liver tissue after laser heating (adapted from Larin <i>et al</i> , 2005).	2
Figure 1.4.1: Schematic showing different type of light detection. (Left) Spherical fibre measuring fluence rate and (right) cleaved fibre measuring radiance within its acceptance cone. 6	6
Figure 1.4.2: Changes in radiance and fluence rate in tissue mimicking phantoms. (a) Radiance sensor facing the light source and (b) radiance sensor facing 180° away from the light source (adapted from Chin et al, 2004).	8
Figure 2.1.1: Optical absorption of various tissue chromophores. Yellow dots show the wavelength of various types of lasers. (http://omlc.ogi.edu/classroom/ece532/class3/muaspectra.html).	11
Figure 2.1.2: Optical absorption of water (left) and temperature-dependent change in water absorption (right) (Matcher <i>et al</i> , 1994, Hollis, 2002).....	12
Figure 2.1.3: Absorption coefficient in native and coagulated porcine liver (Ritz <i>et al</i> , 2001). ..	13
Figure 2.2.1: Temperature-dependent change in the index of refraction of water (left) and silica (right) (Daimon and Masamura, 2007, Toyoda and Yabe, 1983).....	15
Figure 2.3.1: The concept of radiance (L) where Ω represents a solid angle. (http://omlc.ogi.edu/classroom/ece532/class1/radiance.html).	16
Figure 3.1.1: Experimental set-up for water experiments.....	18
Figure 3.1.2: Spectral power output from the white light source (http://www.oceanoptics.com/images/LightSources/hl2000spectra.jpg).	19
Figure 3.1.3: Radiance fibre design showing the the tip of the fibre being cleaved at $\sim 43^\circ$ angle with a protective cap over the tip of the fibre (Fiberoptic Systems Inc. datasheet on left and picture from UPEI on right).	20
Figure 3.1.4:USB4000 spectrometer design (http://www.oceanoptics.com/images/Spectrometers/usb4openbench.jpg).	21
Figure 3.1.5: Relative spectral efficiency of the CCD (left, Toshiba TCD1304AP datasheet) and different gratings (right) available for the USB4000 spectrometer	

(http://www.oceanoptics.com/images/Spectrometers/EfficiencyCurves/gratingeffcurves600.gif).	21
Table 3.2.1: Recovered optical properties of prostate by various investigators. Table is directly taken from Svensson <i>et al</i> (2007).	23
Figure 3.2.1: Experimental set-up. Fibre and thermocouple orientation, looking down at the bottom slab before heating.....	24
Figure 3.2.2: Schematic of the experimental set-up during the heating phase.	24
Figure 3.2.3: Picture of the cylindrical fiber inside the catheter (from Visualase Inc.). Picture from Schwartz <i>et al</i> 2011.....	25
Figure 3.2.4: PDA36A photodiode spectral response (http://www.thorlabs.com/images/TabImages/PDA36A_response_large.gif).	26
Figure 3.2.5: Schematic of the experimental set-up during the cooling phase.	27
Figure 3.3.1: Optical properties in heated and cooled tissue for three different cases.	30
Figure 4.1.1: Raw optical spectra in air (black) and in water (blue).	33
Figure 4.1.2: Ratio of optical radiance signals from air-to-water as an absorption measurement (left axis). The absorption coefficient of water absorption from Matcher <i>et al</i> (1994) is also presented (right axis). Experimental data normalized to 700 nm.	33
Figure 4.1.3: Spectral radiance ratio as a function of temperature from 22°C - 70°C. Experimental data normalized to 700 nm.	34
Figure 4.1.4: Spectral radiance ratio in water (I) relative to water at room temperature before heating (I_{before}) (left axis). The temperature dependent change in the optical absorption coefficient of water (from Hollis 2002) is presented for comparison (right axis). Experimental data normalized to 700 nm.	35
Figure 4.1.5: Relative Radiance as a function of angle away from the light source at 810 nm. ..	38
Figure 4.1.6: Full Width Half Maximum (FWHM) in water before heating, heated water at 68°C, cooled water, and air.	39
Table 4.1.1: Estimated acceptance angles of our plane cut fiber materials and water with 50°C increase in temperature.	39
Figure 4.2.1: Bottom slab of porcine muscle after heating. Coagulated tissue shown as a white colour due to laser heating.	41

Figure 4.2.2: Temperature profile and normalized radiance signal with time starting with the first temperature measurement for experiments using heating protocol i).....	42
Figure 4.2.3: Temperature profile and normalized radiance signal with time starting with the first temperature measurement for experiments using heating protocol ii).....	43
Table 4.2.1: Temperature measurements for experiments using heating protocol i).....	45
Table 4.2.2: Temperature measurements for experiments using heating protocol ii).	45
Figure 4.2.4: Spectral changes where I_{heated} is the first spectrum (heated tissue), I_{cooled} is the last spectrum (cooled tissue) on the left axis compared with Hollis' temperature-dependent change in water absorption of water on right axis. Top graph using experimental protocol i) and bottom graph using protocol ii).....	46
Table 4.2.3: Location of the Temperature-Dependent Optical Absorption Peaks Measured in coagulated <i>ex vivo</i> porcine muscle.....	47
Figure 4.2.5: Raw radiance signals obtained in porcine muscle tissue before heating, immediately after heating and after cooling using heating protocol i).	48
Figure 4.2.6: Raw radiance signals obtained in porcine muscle tissue before heating, immediately after heating and after cooling using heating protocol ii).	49
Figure 4.2.7: Changes in the optical radiance ratio spectrum with time. Colour represents the change $-\ln(I_{heated}/I_{cooled})$, where I_{heated} represents the heated spectrum at a particular time point and I_{cooled} is the last spectrum. Top experiment show results using experimental protocol i) and bottom experiments show results using experimental protocol ii).	51
Figure 4.2.8: Change in the spectrum with time, $-\ln(I_{heated}/I_{cooled})$, at 740 nm, 840 nm and 960 nm normalized to the change found in the first spectrum acquired. Temperature at the radiance fibre is shown on the right axis. Results from experiment #1 using heating protocol ii).....	52
Table 4.3.1: Residual sum of squares between the experiments 1 and 2 using heating protocol i) and the three cases using theoretical radiance calculations for wavelengths of 700 – 1000 nm. .	53
Figure 4.3.1: Theoretical radiance comparison between simulated heated tissue and cooled tissue. Case #1 represents changes due to temperature-dependent water absorption. Case #2 represents temperature-dependent water absorption and a 10% increase in water content. And case #3 represents temperature-dependent water absorption and 10% change in reduced scattering.	54
Figure A.1: Tissue heating experiment using 10 watt laser power. Source-detector distance 1 cm.	60

Figure A.2: Tissue heating experiment using 10 watt laser power. Source-detector distance 1 cm.	61
Figure A.3: Tissue heating experiment using 6 watts laser power with no cooling catheter. Source-detector distance of 5 mm.....	62
Figure A.4: Tissue heating using 8 watts laser power. No cooling catheter. Source detector distance of 5 mm.	63
Figure A.5: Tissue heating experiment using 10 watts laser power with the diomed-15 laser. Source detector distance of 5 mm.	64
Figure A.6: Tissue heating experiment using 12 watts laser power. Source detector distance of 5 mm.	65
Figure A. 7: Tissue heating experiment using 10 watts laser power. Source-detector distance of 5 mm.	66
Figure B.1: Three trials of diffuse reflectance data in native porcine muscle. Theoretical diffuse reflectance in blue fitted to the measured diffuse reflectance in red.	69
Figure B.2: Three trials of diffuse reflectance data in coagulated porcine muscle. Theoretical reflectance in blue fitted to the measured reflectance in red.	70

List of Tables

Table 3.2.1: Recovered optical properties of prostate by various investigators. Table is directly taken from Svensson <i>et al</i> (2007).	23
Table 4.1.1: Estimated acceptance angles of our plane cut fiber materials and water with 50°C increase in temperature.	39
Table 4.2.1: Temperature measurements for experiments using heating protocol i).....	45
Table 4.2.2: Temperature measurements for experiments using heating protocol ii).	45
Table 4.2.3: Location of the Temperature-Dependent Optical Absorption Peaks Measured in coagulated <i>ex vivo</i> porcine muscle.....	47
Table 4.3.1: Residual sum of squares between the experiments 1 and 2 using heating protocol i) and the three cases using theoretical radiance calculations for wavelengths of 700 – 1000 nm. .	53

1 Introduction

1.1 Conventional Cancer Treatments

In Canada, prostate cancer is the most common cancer in men. It is expected that 25,500 new cases of prostate cancer will be presented in 2011 (Canadian Cancer Statistics, 2011). The common methods to treat cancer in general are radiation, chemotherapy and surgery. A problem with some of these cancer treatments is treating large malignant tumours and tumours close to critical organs. Surgery is one viable option; radical prostatectomy is considered the gold standard for localized cancer (Schaeffer *et al*, 2010). However, open surgery is inherently invasive and it can also increase the risk of cancer metastasis (Ben-Eliyahu, 2002). In addition, patients have erectile dysfunction and urinary incontinence following radical prostatectomy (Potosky *et al*, 2004). Chemotherapy involves the intake of drugs systematically and generally affects fast growing cells at a certain cell growth stage depending on the drug. Cancerous cells which proliferate faster than normal cells are affected most. However, it has been shown that chemotherapy for prostate has generally poor response (Shelley *et al*, 2006). In addition, chemotherapy has undesirable side effects such as nausea and hair loss. Radiation therapy uses ionizing radiation beams which damages not only the target tumour but also the proximal tissue. The problems associated with radiation therapy are similar to radical prostatectomy as patients experience erectile dysfunction, urinary incontinence and bowel urgency (Potosky *et al*, 2004). Although these are the conventional methods to treat cancer, it is of great interest to develop and validate new novel cancer treatments that increases patient survival and quality of life.

1.2 Thermal Therapy

Thermal therapy uses heat to treat malignant tumours by heating tissue to high temperatures (55-90°C) for a short period of time (~2-5 minutes). At these high temperatures cell death occurs due to coagulative necrosis. Two major effects take place during this process. The first is the weakening of the cell membrane wall due to heat. The cell membrane wall is composed of a bilipid layer where the inter portion is composed of hydrophobic lipids held together by hydrogen bonding. During heating, the hydrogen bonds weaken causing the cell membrane to expand. The leakage of intercellular and extracellular fluids causes the cell to stop functioning properly and die. The second effect is the thermal denaturation of proteins. Proteins

have an inherent structure, during the denaturation process proteins unfold and lose their function and structure. Tissue appears to be white after heating due to the loss of structure in proteins on a large scale. Coagulative thermal therapy differs from a similar type of therapy called hyperthermia where temperatures between 43-50°C are achieved for longer periods of times (~1 hour). These lower temperatures disrupt cell physiological functions and enzyme production similar to the effect of the weakening of the cell membrane which leads to cell death (Pearce and Thomson, 1995). Tissue ablation differs from coagulative thermal therapy by heating tissue to temperatures above 100°C, vaporizing the tissue. This has most commonly been done using lasers such as Holmium Yttrium Aluminum Garnet (Ho:YAG) at a wavelength of 2,100 nm. At this wavelength high temperatures are generated due to the absorption of light due to water. This has been used to treat urethral stricture (Sun *et al*, 2006).

During thermal therapy, there is an immediate effect of cell death due to tissue coagulation closest to the heating source and a latent effect in cell death caused by lower temperatures further away from the heating source. Latent cell death, which is not immediately visible, can occur between a few hours and up to two days. Figure 1.2.1 shows an example of a thermal lesion in canine liver where the white region is the coagulated tissue due to thermal damage.

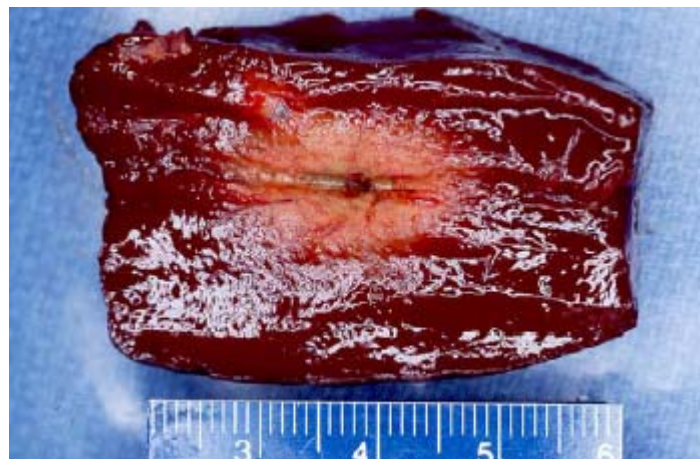


Figure 1.2.1: Gross picture of canine liver tissue after laser heating (adapted from Larin *et al*, 2005).

Various heating sources have been used for such a treatment ranging in its invasiveness. High intensity focused ultrasound (HIFU) is a non-invasive heating technique where the transducer is placed outside the body (Wu *et al*, 2003). Specialized probes exist such as transrectal ultrasound probes to treat prostate (Inoue *et al*, 2011). Other techniques are minimally-invasive such as microwave therapy which employs placing antennae into the target (Sherar *et al*, 2003). Gold nanoparticles and paramagnetic particles can be injected into the tumour and excited using a laser (Schwartz *et al*, 2011) or external magnetic field (Konishi *et al*, 2004), respectively, to generate localized heat inside the tumour.

Laser interstitial thermal therapy (LITT), the focus of this thesis, is a minimally invasive heating modality in which optical fibres are inserted into the target tumour with the imaging guidance of either ultrasound or magnetic resonance imaging (MRI) (Bown 1983, Quesson *et al*, 2000, Garcia-Medina *et al*, 2011). Two examples of commercial systems are the Visualase system by Visualase Inc. and the Indigo laser system by Ethicon Endo-Surgery Inc. A cylindrical diffuser is commonly used to treat large malignancies because it can deliver a higher power of light over a larger volume compared with a spherical tipped fibre or plain cut fibre. In other words a cylindrical fiber is a larger light source and therefore a larger heat source. Due to their flexibility, the fibres are placed inside a rigid catheter. The optical fibre is attached to a high powered laser. Heat is generated by the absorption of non-ionizing light typically in the near-infrared (NIR) by chromophores. Depending on the wavelength chosen for the procedure and the optical properties of the tissue, different heating times and volumes of damage can be achieved. Using a 980 nm diode laser, powers between 0.5 – 30 watts have been used *in vivo* (McNichols *et al*, 2004, Garcia-Medina *et al*, 2011). At a wavelength of 1,064 nm, Neodymium-doped Yttrium Aluminum Garnet (Nd:YAG) laser with powers of 0.5-80 watts have been used (Hillegersberg *et al*, 1994). Some LITT treatments use a cooling catheter surrounding the fiber, which are designed to allow the flow of water around the fibre to create a cooling effect. This cooling has two effects. First it prevents the fiber from reaching high temperatures that would normally damage the fibre. Secondly, it affects the temperature distribution in the tissue. Without the use of a catheter the peak temperature is proximal to the heating fibre. When using a cooling catheter the peak temperature is pushed further into the tissue. This is considered a safe approach for patient treatment because the cooling of the fibre reduces the risk of reaching temperatures above 100°C at the fibre and possibly charring the tissue (Carpentier *et al*, 2008). Tissue charring

leads to a high absorption barrier around the fibre causing a large increase in heat which can potentially damage the fibre. Also, tissue charring can limit the light delivery to the target tissue and affect the outcome of the treatment.

Thermal dose is commonly used to evaluate thermal damage due to heat. Thermal damage in tissue is dependent on both temperature and time. Henriques was the first person to show the temperature-time relationship of thermal damage in tissue and modeled the damage as an Arrhenius rate process (Henriques, 1947). The model shows how different treatment times with different temperatures can achieve the same final thermal damage. As mentioned before, thermal damage may appear to be different some time post treatment due to latent thermal damage. The thermal dose model attempts to include these latent effects.

1.3 Real-Time Monitoring of LITT

The goal with thermal therapy, as with other cancer treatments, is to treat the diseased tissue while sparing the proximal healthy tissue. One problem with LITT is that there exists a temperature gradient away from the heat source; the highest temperature being closest to the heating source. This introduces the risk of tissue charring at the heating fibre. Other confounding factors are blood flow which affects LITT in two opposing ways: 1) it creates an increase in absorption causing more heat generation and 2) it cools the tissue by carrying heat away. As a result, response to a standard treatment can vary between patients. Because of this variation between patients, monitoring the treatment in real-time is important to ensure a successful treatment of the entire target tumour with either minimal or no damage to the proximal healthy tissue. Various monitoring methods have been investigated such as magnetic resonance imaging (MRI), thermometry with thermal damage models, ultrasound imaging, optoacoustic imaging and optical techniques.

Thermocouples or fluoroptic probes are the simplest method to measure temperature at discrete locations. However, there are two problems with this technique. First, these temperature measurements are discrete and require the insertion of multiple probes to acquire spatial temperature measurements. This increases invasiveness of the treatment. Multiple spatial measurements are necessary especially close to the heating source where the temperature is highest to prevent the risk of tissue charring. Studies have shown overestimation in temperature when placing a thermocouple close to the heating fibre due to the absorption of light by the

thermocouple (Reid *et al*, 2001). Second, it is difficult to assess tissue damage based on temperature alone, therefore it is necessary to couple temperature information with a thermal damage predicting model (Sapareto and Dewey, 1984).

MRI can be used in two ways to monitor LITT. One of these methods involves using MRI data to detect structural changes due to thermal damage (Tracz *et al*, 1993). The second method involves using MRI to acquire a three dimensional temperature map of the target tissue (Quesson *et al*, 2000, Garcia-Medina *et al*, 2011). This information can be coupled to a thermal damage model to predict tissue damage. An inherent problem during MRI monitoring is the introduction of artefacts due to patient movement. Also, MRI is expensive and are not readily available, limiting its clinical use.

Ultrasound is less expensive and more readily available compared to MRI. The investigations conducted in the monitoring of thermal therapy have shown that it is not effective at discriminating the entire coagulated volume real-time compared with native tissue due to the formation of bubbles (Gertner *et al*, 1997). Optoacoustic technology is being investigated in monitoring thermal therapy. This technique is based on the emission of ultrasound waves from tissue due to thermal expansion caused by the absorption of light. Arsenault *et al* (2009) and Chitnis *et al* (2011) have shown it can potentially be used in monitoring thermal therapy.

1.4 Optical Monitoring of LITT

Optical monitoring measures changes in light intensity as light passes through the target treatment region during LITT. It is most useful in conjunction with LITT because the optical fibre used to heat the tissue can also be used as the source of the signal during the monitoring of the treatment. Tissue optical properties change due to thermal damage (Cheong 1995, Whelan and Wyman, 1999, Skinner *et al*, 2001) and in particular the optical scattering causing the optical signal to change due to a different light attenuation. An example of the changes due to thermal damage found in the reduced scattering coefficient in porcine liver is 3.85 cm^{-1} in native tissue to 38 cm^{-1} in coagulated tissue at 830 nm (Ritz *et al*, 2001). In human liver the reduced scattering changed from 9.18 cm^{-1} in native tissue to 26.67 cm^{-1} in coagulated tissue at 850 nm (Germer *et al*, 1998).

Fluence rate and radiance measurements have been investigated for monitoring LITT (Chin *et al*, 2004). Fluence rate measurements use spherically tipped fibres which measure light from all directions. Radiance measurements use optical fibres cleaved at an angle (typically $\sim 43^\circ$). The concept in detection using a cleaved fibre is that the light enters the fibre and reflects off the hypotenuse due to the mismatch in the index of refraction of the medium and fiber. Figure 1.4.1 shows how fluence rate can be detected using a spherically tipped fibre and radiance using a cleaved fibre. If the light enters the fibre within its acceptance cone it is reflected into the fibre and detected. The hypotenuse can be coated with a reflective material increasing the collection efficiency of the fibre and decreasing the optical signal coming through the hypotenuse. The purpose of using cleaved fibres instead of plain cut fibre is that cleaved fibres can be inserted into tissue from the same direction as the source fibre. With the fibre cleaved at an angle the fibre can collect light perpendicular to the direction in which it was inserted and can be rotated to gather light from another direction. To acquire the same measurement using a plain cut fibre the fibre would need to be inserted perpendicular to the direction the light source was inserted into tissue. This can be difficult to achieve due to other proximal organs and access points. In addition, a plain cut fibre cannot be rotated in the same manner as a fibre cleaved at an angle.

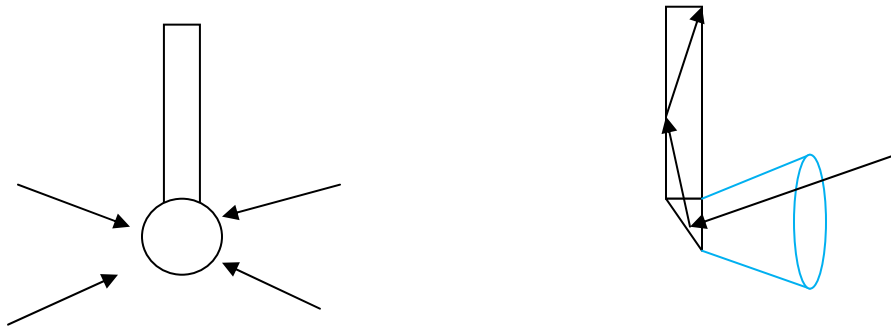


Figure 1.4.1: Schematic showing different type of light detection. (Left) Spherical fibre measuring fluence rate and (right) cleaved fibre measuring radiance within its acceptance cone.

Both fluence rate and radiance are point measurements but changes in their signal represent changes to a particular volume. Chin *et al* (2004) have reported that radiance measurements are much more sensitive than fluence measurements to the changing optical properties of tissue due to thermal damage during LITT experiments, as shown in Figure 1.4.2.

Using a cylindrically diffusing optical fibre coupled to a laser for heating and measuring radiance facing the source, the signal decreased by 60% at which point the coagulation had reached the detector. The change in signal was due to the increase in scattering of light in the coagulated tissue region. The increased scattering causes light to travel a longer distance as it diffuses away from the light source. This causes more light to be absorbed before reaching the detector. As the coagulated region extends past the detector more light scatters back towards the sensor and the optical signal increases. When the collection fibre was oriented away from the light source, the optical signal increased by a factor of 2 as the coagulation boundary passed the detector. The increase in scattering from the coagulated tissue causes light to scatter back into the detector, increasing the optical signal (Chin *et al*, 2007).

This use of measuring relative changes in the optical signal is advantageous in the context of monitoring LITT because the optical properties of the same organ (such as prostate) vary between patients. Svensson *et al* (2007) had recovered reduced scattering coefficients between 4.5 and 10.1 cm^{-1} between patients, a percent difference of over 100%. It is difficult to assess tissue damage based on absolute optical property measurements because each patient may have different optical properties before treatment.

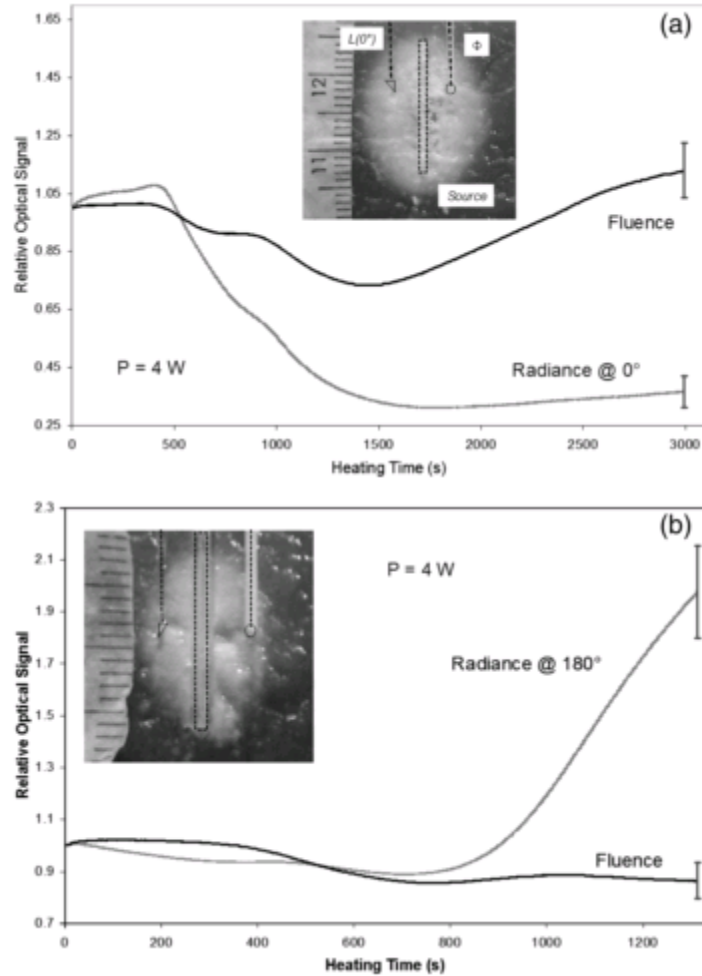


Figure 1.4.2: Changes in radiance and fluence rate in tissue mimicking phantoms. (a) Radiance sensor facing the light source and (b) radiance sensor facing 180° away from the light source (adapted from Chin et al, 2004).

1.5 Project Overview

Radiance measurements have been shown to detect dynamic changes in optical propagation with heating time and temperature. However, previous studies have not thoroughly investigated if these optical changes in the radiance signal during LITT are permanent caused by thermal damage or if the optical signal changes observed after heating are influenced by a temperature based transient change in optical propagation of tissue during cooling.

The hypothesis of the project is:

Radiance signals measured during the monitoring of LITT represent a permanent change in tissue due to thermal damage. To assess this hypothesis the specific aims of the project are:

- 1) Develop a radiance detection system and test its sensitivity by measuring the optical absorption spectrum and the temperature-dependent optical absorption spectrum of water.
- 2) Test if the radiance system materials exhibit a temperature-dependent perturbation in optical detection.
- 3) Monitor radiance during the cooling of *ex vivo* tissue immediately following laser heating in the tissue and assess the representation of the radiance signal.

2 Theory

2.1 Optical Properties of Tissue

The Beer-Lambert equation (equation 2.1) is commonly used to describe the attenuation of light in a purely absorbing medium using the following:

$$I = I_o e^{-\mu_a x}, \quad (2.1)$$

where I represents the amount of light exiting a medium, I_o represents the light entering the medium, μ_a represents the absorption coefficient and x represents the optical path length. The equation assumes a collimated light source and detector. This shows that the intensity of light decays exponentially in a purely absorbing medium. However, tissue is not purely absorbing but rather contains scatterers that cause the direction of light to change and increase the path lengths to the detector. As a result, equation 2.1 cannot be applied to tissue but rather describes the attenuation with distance as an exponential decay.

The absorption coefficient (μ_a [cm^{-1}]) of tissue depends on tissue chromophore composition, concentration and wavelength. The major chromophores of tissue are water, oxyhemoglobin and deoxyhemoglobin. Tissue is typically composed of 75% water. Both water and blood (which is a combination of oxyhemoglobin and deoxyhemoglobin) absorb red and near-infrared (NIR) light least. This allows light to propagate further into tissue allowing energy deposition further from the heat source rather than relying solely on the diffusion of heat. In addition, allowing light to propagate further in tissue introduces the possibility of detecting light for diagnostic purposes. Figure 2.1.1 shows the various chromophores found in tissue.

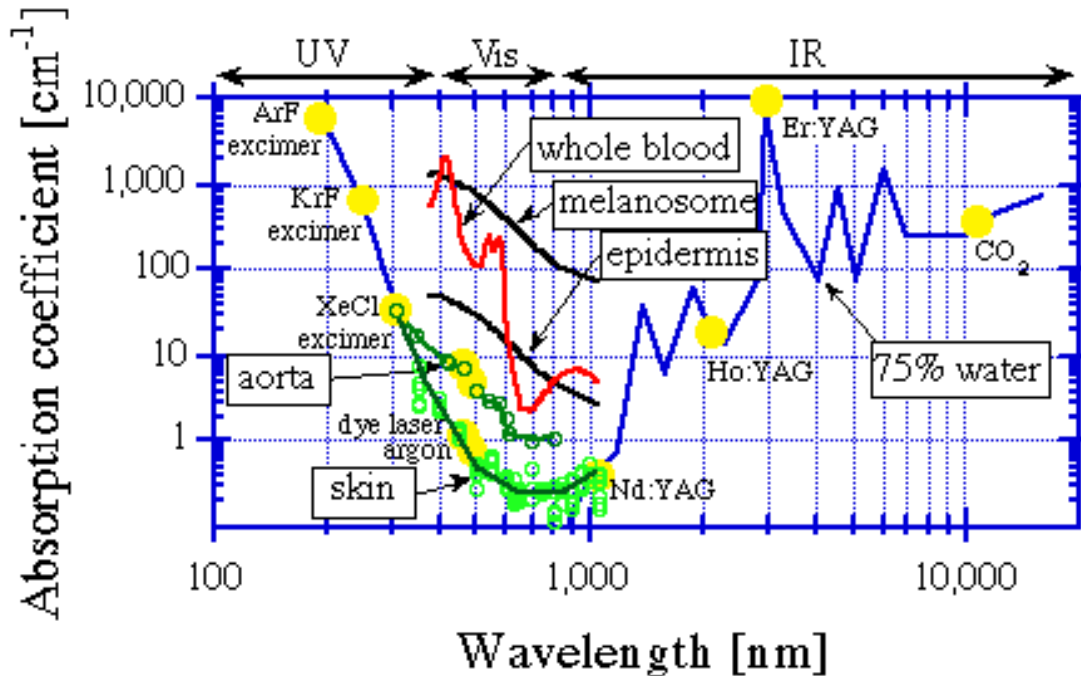


Figure 2.1.1: Optical absorption of various tissue chromophores. Yellow dots show the wavelength of various types of lasers. (<http://omlc.ogi.edu/classroom/ece532/class3/muaspectra.html>).

The absorption spectrum of water varies with temperature as reported by Collins in 1925 and more recently Hollis (2002) and Langford *et al* (2001). The most notable features in the temperature-dependent spectrum of water are increases in absorption at wavelengths of 739 nm, 837 nm and 962 nm. Figure 2.1.2 shows the absorption of water and its change in absorption with temperature in the NIR region. The changes in the absorption are due to the first overtone of the OH stretch (Langford *et al*, 2001). Recently investigators have observed that the temperature-dependent changes of water in a turbid media can be detected (McGlone *et al*, 2007, Cletus *et al*, 2010, Chung *et al*, 2010). The importance of these studies is that the temperature-dependent changes in water may affect the measured optical signals in tissue.

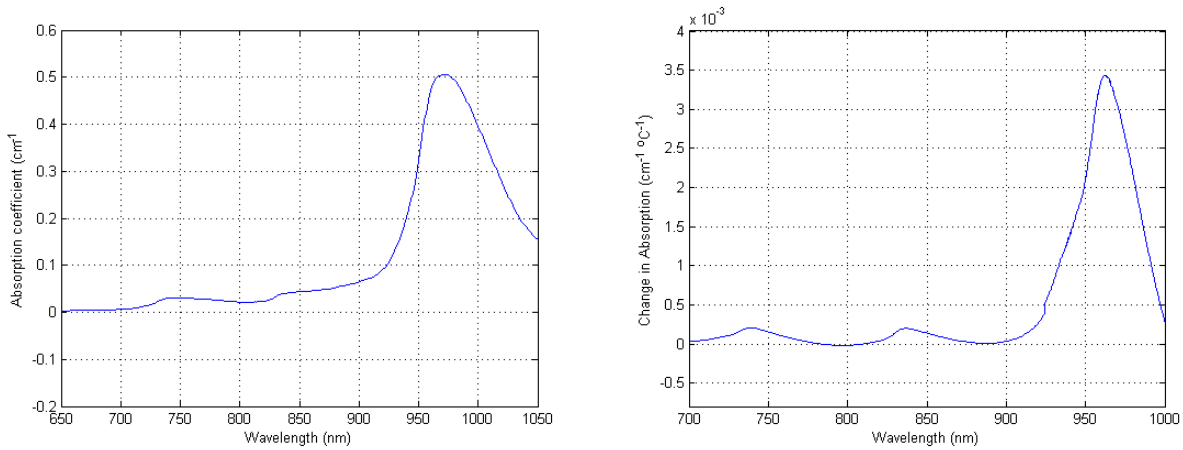


Figure 2.1.2: Optical absorption of water (left) and temperature-dependent change in water absorption (right) (Matcher *et al*, 1994, Hollis, 2002)

Optical scattering (μ_s [cm^{-1}]) in tissue is due to the cells and its organelles. The cell's nucleus contributes the most to scattering due its size but other smaller cell organelles also contribute to the total scattering. In addition, collagen and the cell membrane is a major contributor to the scattering of light. In the NIR regime most scattering can be described by a distribution of various sizes. The reduced scattering, μ'_s , is similar to the scattering coefficient but takes into account the preferential direction of scattering in tissue based on the anisotropy factor. The reduced scattering can be described over a spectrum using a power law equation (Mourant *et al*, 1997),

$$\mu'_s(\lambda) = \mu'_s(\lambda_o) \left(\frac{\lambda}{\lambda_o}\right)^{-b}, \quad (2.2)$$

where μ'_s is the reduced scattering at a wavelength of λ , $\mu'_s(\lambda_o)$ is the reduced scattering coefficient at a reference wavelength of λ_o and b is related to the average scatterer size. This indicates that scattering decreases gradually with increasing wavelength in the visible and NIR spectrum.

Changes in optical scattering are permanent following LITT due to thermal damage. At temperatures between 55°C and 90°C protein denaturation occurs causing tissue to coagulate (Pearce and Thomson, 1995). Coagulated tissue is observed as whitening of the tissue. This biological effect increases the reduced scattering coefficient by 2-10 times its original value

(Germer *et al*, 1999, Whelan and Wyman, 1999, Skinner *et al*, 2000, Ritz, *et al*, 2001). Unlike the temperature-dependent change in water absorption, which is reversible, the changes in scattering are mainly permanent. However, some data in tissue mimicking phantoms suggests there may be a temperature-dependent change in scattering (Cletus *et al*, 2010). In that study, the temperature-dependence in scattering was due to a change in the indices of refraction of the water and Intralipid. Permanent changes in optical absorption due to LITT have not been well characterized. Absorption can decrease due to tissue dehydration or increase because of charring when tissue reaches higher temperatures ($>100^{\circ}\text{C}$). Figure 2.1.3 shows different changes in absorption in the visible and NIR spectrum in native and coagulated porcine liver. More specifically, the changes in the absorption coefficient due to coagulation between 400 and 900 nm had increased while in the 840 nm to 1350 nm range the absorption coefficient had decreased with coagulation.

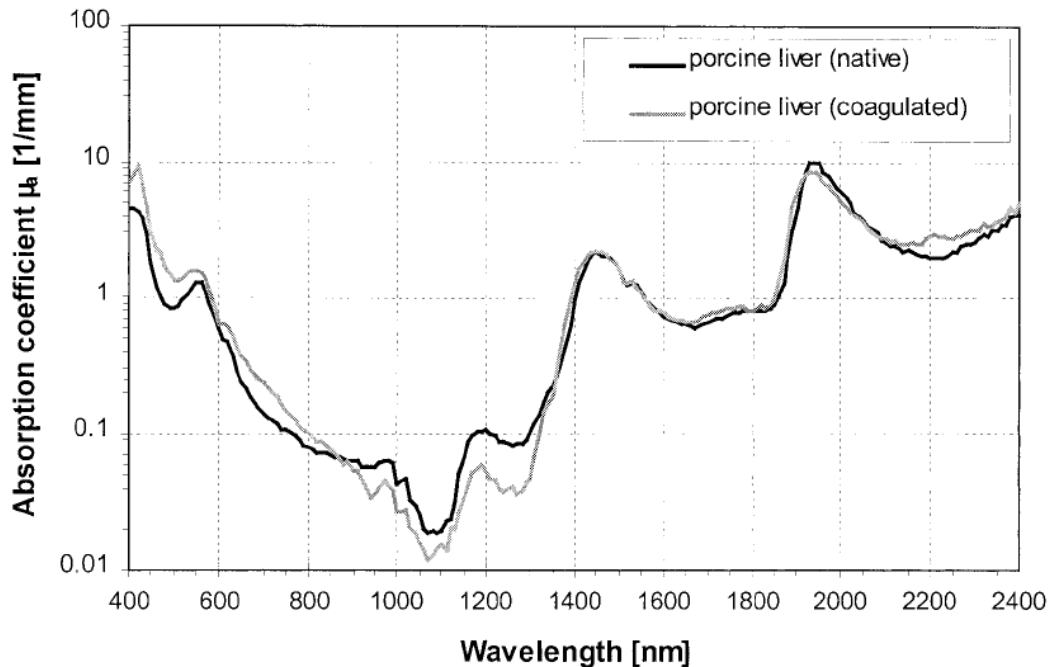


Figure 2.1.3: Absorption coefficient in native and coagulated porcine liver (Ritz *et al*, 2001).

2.2 Index of Refraction

The index of refraction of the medium and material fiber is used to determine the numerical aperture of the fiber. The numerical aperture (NA) is related to the full width half

maximum which describes the angle at which over 50% of the light is detected in a given medium (typically in air). The numerical aperture is defined as:

$$NA = n \sin\theta, \quad (2.3)$$

where n represents the index of refraction of the medium and θ represents the maximum angle at which photons can be detected. NA can also be calculated using the indices of refraction of the core and cladding of the optical fiber:

$$NA = \sqrt{n_1^2 - n_2^2}, \quad (2.4)$$

where n_1 and n_2 are the indices of refraction of the core and cladding respectively.

The index of refraction of water exhibits a reversible temperature-dependent change, decreasing in the visible and NIR spectrum of water as temperature increases (Daimon and Masamura, 2007). The index of refraction of silica (the primary component of the optical fibre) increases with an increase in temperature (Toyoda and Yabe, 1983). The changes in water and silica are opposite. However, the change in the index of refraction of water is dominant (~8 times greater than silica). Figure 2.2.1 shows the spectral change in the index of refraction due to temperature of water and silica.

The increase mismatch in the indices of refraction between the medium (water) and the detector (silica) affects the signal in two ways: 1) it increases Fresnel reflections and 2) it increases the angle at which light can enter the fibre (full width half maximum).

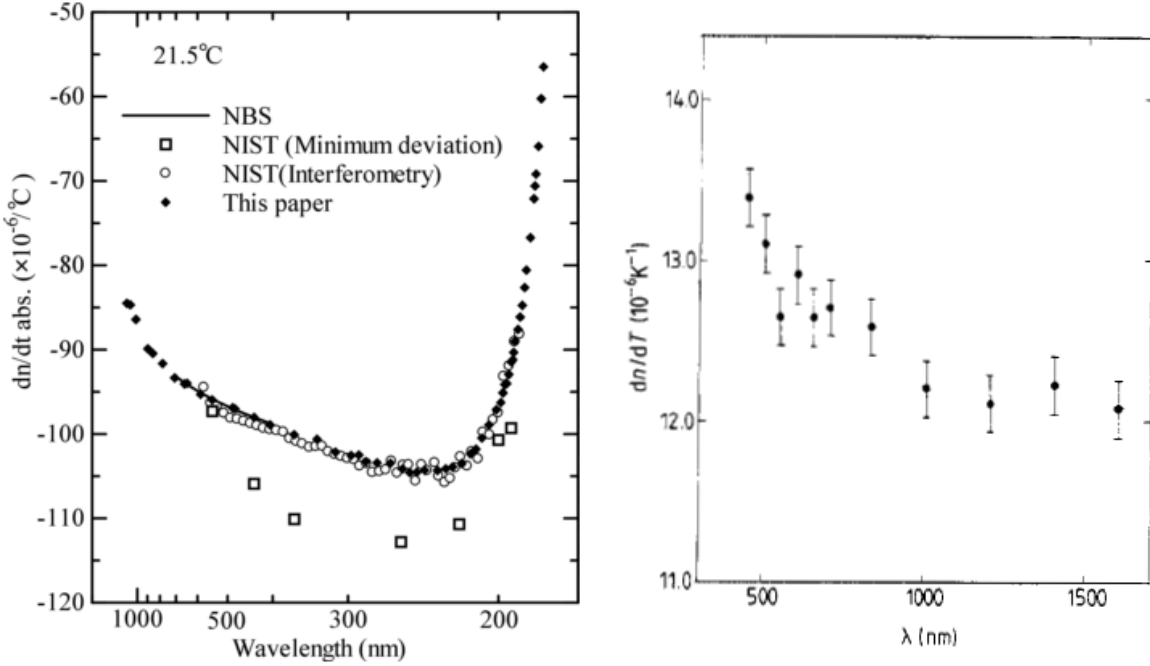


Figure 2.2.1: Temperature-dependent change in the index of refraction of water (left) and silica (right) (Daimon and Masamura, 2007, Toyoda and Yabe, 1983).

2.3 Radiative Transport

The radiative transport equation (Equation 2.5) describes the propagation of light in a medium which can contain both absorption and scattering, referred to as a turbid medium. Light is described as photon particles. As these particles propagate through tissue they are either absorbed or scattered in another direction. The anisotropy factor describes which direction most photons scatter (i.e., forward or backward). The reflections and refraction of light between tissue constituents depends on the index of refraction. Hence the main properties describing light propagation in tissue are: the absorption coefficient, scattering coefficient, anisotropy factor and the index of refraction. One form of the radiative transport equation that describes the above interactions is the following:

$$\frac{dL(r, \hat{s})}{ds} = -\mu_a L(r, \hat{s}) - \mu_s L(r, \hat{s}) + \mu_s \int_{4\pi} p(s, \hat{s}') L(r, \hat{s}') d\omega' + S(r, \hat{s}), \quad (2.5)$$

The first term describes the change in radiance per area. The second and third terms describe the changes due to absorption and scattering. The fourth term describes the increase in radiance due to scattering. The term $p(s, \hat{s})$ is a phase function describing the direction which photons preferentially scatter. And the last term is the light due to the optical source.

Radiance is a measure of power (P) per unit area (A) per steradian (sr), where a steradian is a solid angle. Figure 2.3.1 illustrates the concept of radiance and solid angles.

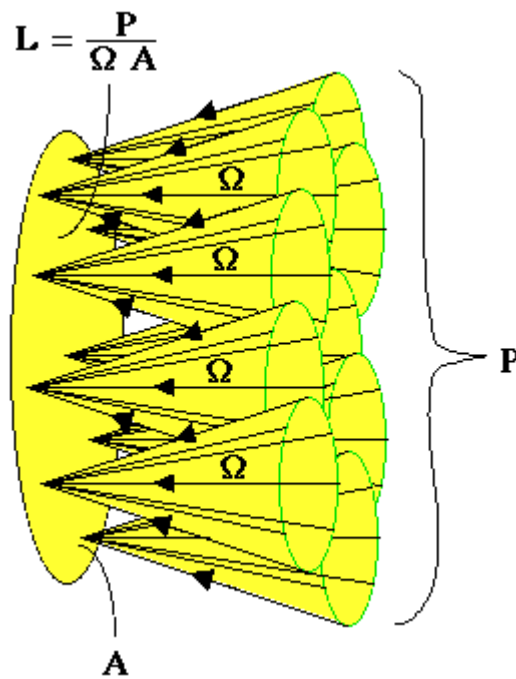


Figure 2.3.1: The concept of radiance (L) where Ω represents a solid angle. (<http://omlc.ogi.edu/classroom/ece532/class1/radiance.html>).

Due to the difficulty in solving the radiative transfer equation analytically in complex geometries, Monte Carlo simulations are commonly used to solve problems related to the propagation of light in tissue following the rules of radiative transport. These simulations are statistical in nature and are based on simulating large amounts of photon packets. Recently, an analytical solution to the radiative transfer equation for radiance has been derived using a 17th order legendre polynomial (Liemert and Kienle, 2011).

3 Materials and Methods

This section describes the radiance detection system and how it was used to assess the main hypothesis. The radiance system consists of an optical fibre cleaved at an angle connected to a detector (spectrometer or photodiode). The optical signal was generated either by a non-heating white light source or a heating diode laser. All experiments were conducted in a dark room to reduce background noise in the acquired signal.

3.1 Experiment #1: Measurements in Water

To test the radiance detection system, water heating experiments were conducted to determine if the sensitivity of the radiance system is able to detect small changes in the optical spectrum. Figure 3.1.1 shows the optical fibres being guided into the phantom container using metal tubing. The spherical source fibre is fixed using an acrylic jig and the radiance fibre is mounted to a rotational stage. The source-detector distance is 1 cm.

Radiance measurements of water were chosen because water is a significant component of tissue and, as noted earlier, has a temperature dependent absorption spectrum which has been reported in literature. Experimental data was compared with the spectra acquired from *Matcher et al* (1994) and *Hollis* (2002) due to the availability of the spectra as a text file. The water absorption data used was the optical absorption of water at 37°C by *Matcher et al* (1994) and temperature-dependent optical absorption by *Hollis* (2002). Their respective spectra are shown in figure 2.1.2.

A copper phantom container was chosen because copper conducts heat well therefore reducing the time required to heat the water. The container was painted black on the inside to reduce reflections from the surface and was filled with water and placed inside a water bath.

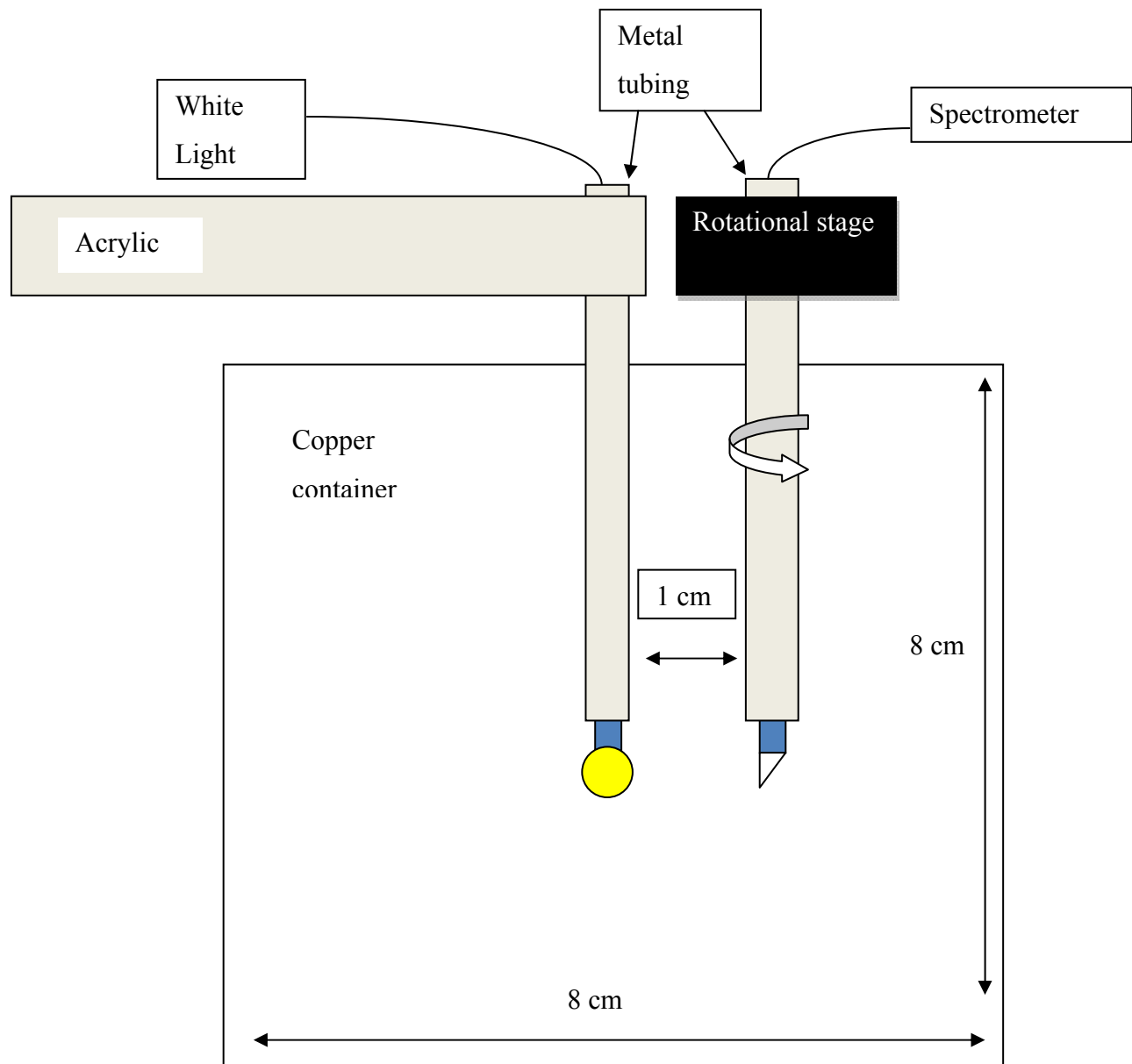


Figure 3.1.1: Experimental set-up for water experiments.

A non-heating tungsten halogen white light source (HL-2000, Ocean Optics, Florida, USA) is used for diagnostic purposes. It is designed to output light efficiently in the visible and NIR region (360 nm – 2000 nm). The output power increases with wavelength in the 360 nm – 1000 nm range as shown in figure 3.1.2. The light source is connected to a spherical diffuser with a core diameter of 400 μm (850 μm outer diameter tip) (IP85, Medlight, Lausanne, Switzerland) using a SMA 905 connector.

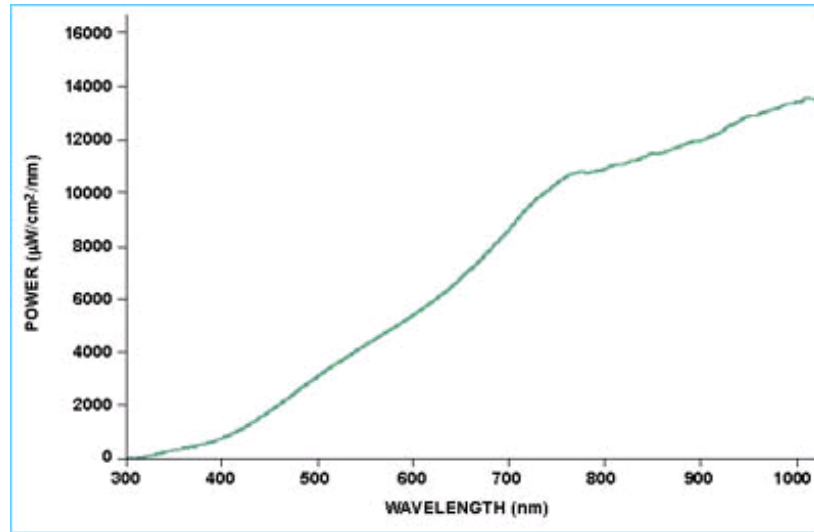


Figure 3.1.2: Spectral power output from the white light source (<http://www.oceanoptics.com/images/LightSources/hl2000spectra.jpg>).

A 500 μm core diameter radiance fibre (Fiberoptic Systems Inc., California, USA) made of silica is used as the detection fibre. These fibres are designed to collect light from the direction they are facing. The fibre is cleaved at $\sim 43^\circ$ with no coating on the hypotenuse therefore causing some light to leak. Figure 3.1.3 shows tip of the fibre is protected from being scratched with a silica cap, however, this can also cause additional reflections. Inside the capillary a vacuum or air exists. It is designed such that the greatest difference in the index of refraction at the hypotenuse exists to reflect light at that location and into the fibre. The radiance fibre was glued to a metal tubing using epoxy to protect the fibre from the risk of breaking when mounting the fibre to a motorized rotational stage (PRM1Z8E, Thorlabs, New Jersey, USA). The rotational stage was used to position the fibre to face the spherical light source.

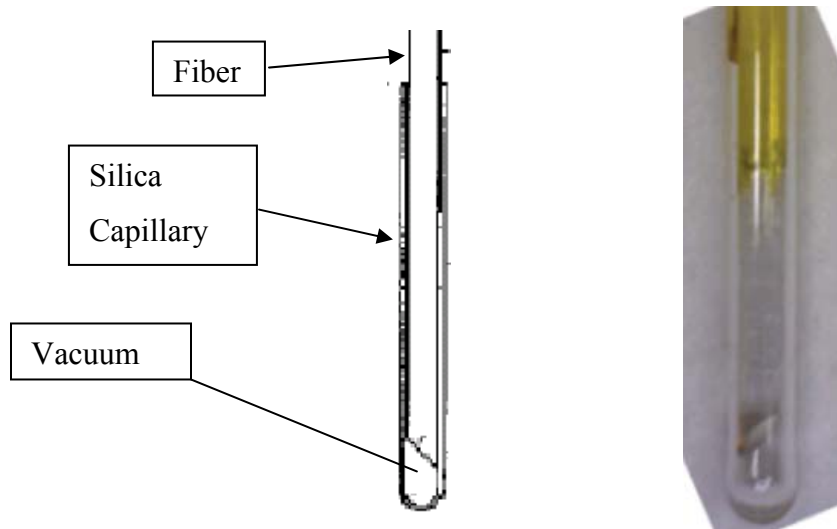


Figure 3.1.3: Radiance fibre design showing the the tip of the fibre being cleaved at $\sim 43^\circ$ angle with a protective cap over the tip of the fibre (Fiberoptic Systems Inc. datasheet on left and picture from UPEI on right).

The radiance fiber was then connected to a spectrometer using a SMA 905 connector. A spectrometer (USB4000, Ocean Optics, Florida, USA) efficient in the visible-NIR is used to acquire spectra throughout the project. It uses a silicon charge-coupled device (CCD) composed of 3648 elements. The spectrometer is based on a crossed Czerny-Turner interferometer set-up using a holographic grating to separate light based on wavelength and a mirror to focus the light onto a detector as shown in figure 3.1.4. Each pixel on the CCD corresponds to a particular wavelength of light. A slit is placed at the entrance of the spectrometer which affects the detection in two ways: 1) it limits the amount of light entering the spectrometer and 2) it affects the pixel resolution of the spectrometer. The spectrometer does not detect the exact output of the white light source, due to its inherent design, but a combination of the source output power, the configuration of the spectrometer and efficiency of the optical fibres being used. Figure 3.1.5 shows the spectral efficiency of the CCD and the relative spectral efficiency of different gratings. A spectrometer with grating #4 was used which has peak efficiency at 750 nm, groove density of 600 and spectral range of 625 nm. The spectrometer contains an entrance slit width of $50 \mu\text{m}$ which has a pixel resolution of 11.6 pixels. The optical resolution is calculated using the following equation:

$$\text{Optical resolution} = \frac{\text{spectral range}}{\text{number of detector elements}} \times \text{pixel resolution} \quad (3.1)$$

inputting all the variables described above results in an optical resolution of ~2 nm.

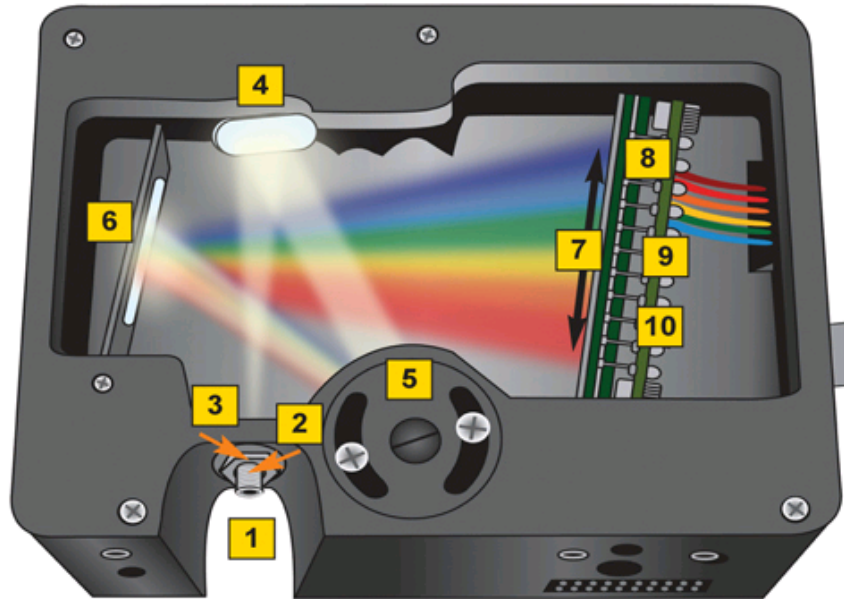


Figure 3.1.4: USB4000 spectrometer design (<http://www.oceanoptics.com/images/Spectrometers/usb4openbench.jpg>).

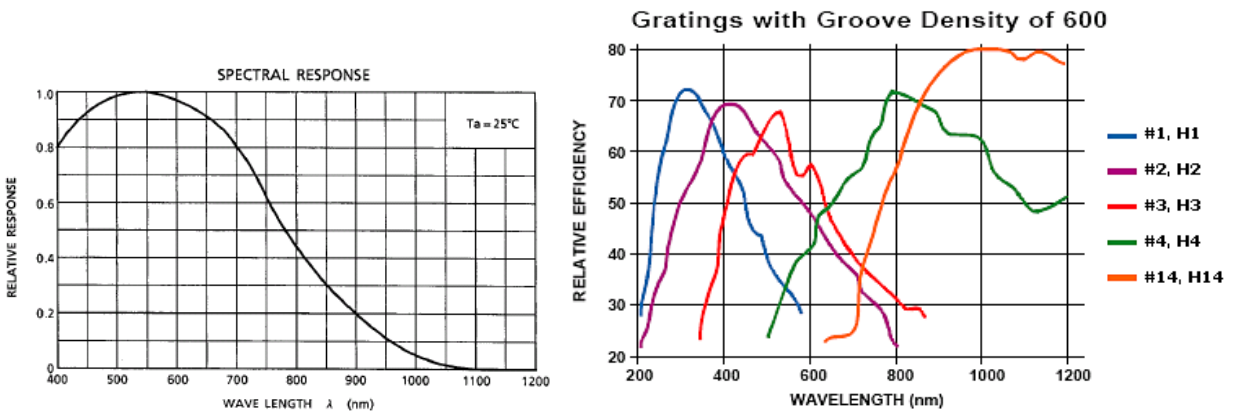


Figure 3.1.5: Relative spectral efficiency of the CCD (left, Toshiba TCD1304AP datasheet) and different gratings (right) available for the USB4000 spectrometer (<http://www.oceanoptics.com/images/Spectrometers/EfficiencyCurves/gratingeffcurves600.gif>).

The following settings were used for acquisition for all experiments in water: integration time of 50 ms, an average of 10 spectra, a boxcar filter of 4 and electric dark correction turned on. The integration time was varied to acquire a strong signal without saturation. The boxcar filter averages the center point and 4 points on each side of a particular data point in question to have reduced noise in the data. The electric dark correction removes a dc like offset in the spectrum. Water was first boiled in a kettle and then transferred to the copper container after it had cooled below 80°C as this is the maximum temperature the radiance fibres can operate according to manufacturer specifications. Preheating the water helps in removing bubble formation during heating which can cause an increase or decrease in the optical signal due to scattering. While the water was inside the phantom container, water was heated to a maximum temperature of 70°C and a spectrum was acquired as the water cooled every 10°C intervals. Temperature was measured before and after each acquired spectrum.

To examine the role temperature changes have on the indices of refraction of silica and water and hence on the fibre's acceptance angle, one experiment measured spectra as the probe was rotated through 360°. A Labview program was created to control the rotational stage and spectrometer to acquire spectra at different angles. Although the motorized rotational stage has a rotational resolution of 0.5° a spectrum was acquired every 1°. Full acquisition of 360° data took ~6 minutes. Temperature was measured before and after data acquisition. The data was post processed in Matlab. The Matlab program implemented boxcar filter of 4. The full width half maximum was found by measuring the angle at which over half the maximum signal was detected. This was done by first finding the angle with maximum intensity and the points at 50% of the maximum normalized intensity. Due to the angular data acquired, the system is not capable of acquiring an exact angle at which exactly 50% of the maximum signal is detected. Using linear interpolation the angle that gives 50% of the maximum intensity was found based on the two closest points.

3.2 Experiment #2: Measurements in *Ex Vivo* Tissue

To assess the hypothesis in a setting that simulates a clinical scenario *ex vivo* laser heating experiments were conducted on slabs of *ex vivo* pork loin tissue. Pork loin was chosen because it was hypothesized that its optical properties match prostate closest. Limited data exists for the optical properties of porcine muscle in the NIR. At 633 nm recovered optical absorption and

reduced scattering coefficients of thawed porcine muscle are 1 cm^{-1} and 1.2 cm^{-1} respectively. While in freshly excised porcine muscle recovered absorption coefficient and reduced scattering coefficients at 633 nm varied from $0.59\text{-}1.2 \text{ cm}^{-1}$ and $24.7\text{-}62.1 \text{ cm}^{-1}$ respectively (Cheong *et al*, 1993). The optical properties of prostate at various wavelengths including in the NIR region are shown in a table from Svensson *et al* (2007) in table 3.2.1.

Table 3.2.1: Recovered optical properties of prostate by various investigators. Table is directly taken from Svensson *et al* (2007).

Study	Description	λ (nm)	N	μ_a	μ_s'	μ_{off}
Pantelides <i>et al.</i> ²⁴ (1990)	<i>ex vivo</i> steady state data, normal whole prostates	633	3	0.7 ± 0.2	8.6 ± 0.5	4.3 ± 0.5
Whitehurst <i>et al.</i> ²⁶ (1994)	<i>in vivo</i> steady state data, untreated BPH and PC	633	11			3.6 ± 0.2
Lee <i>et al.</i> ²⁸ (1995)	<i>in vivo</i> steady state data, untreated BPH and PC	633	11			3.9 ± 0.5
Lee <i>et al.</i> ²⁸ (1995)	<i>in vivo</i> steady state data, untreated BPH and PC	665	11			3.2 ± 0.5
Lee <i>et al.</i> ²⁹ (1999)	<i>in vivo</i> steady state data, untreated PC	630	7			3.5 ± 0.7
This study	<i>in vivo</i> time-resolved data, untreated PC	660	9	0.5 ± 0.1	8.7 ± 1.9	3.6 ± 0.8
Weersink <i>et al.</i> ³⁰ (2005)	<i>in vivo</i> steady state data, recurrent PC	762	22	0.4 ± 0.2	3.4 ± 1.6	2.0 ± 0.6
Zhu <i>et al.</i> ³⁴ (2005)	<i>in vivo</i> steady state data, recurrent PC	732	13	0.4 ± 0.2	11.8 ± 8.2	3.3 ± 0.5
This study	<i>in vivo</i> time-resolved data, untreated PC	786	9	0.4 ± 0.1	7.1 ± 1.6	2.9 ± 0.7
This study	<i>in vivo</i> time-resolved data, untreated PC	916	9	0.6 ± 0.1	7.7 ± 1.8	3.8 ± 0.8
Essenpreis <i>et al.</i> ²⁵ (1992)	<i>ex vivo</i> integrating sphere data, normal prostates	1064		1.5 ± 0.2	6.4	

The set-up consisted of two slabs of tissue held in a plastic plate to minimize tissue movement during heating as this can cause the fibres to become misaligned. A source detector distance of 5 mm was chosen to ensure that the region of coagulation passes the detector. The optical fibres were mounted horizontally and aligned on top of the bottom slab. Figure 3.2.1 shows the cylindrical diffuser inside the cooling catheter and the placement of the radiance fibre 5 mm from the center of the cylindrical diffuser. Thermocouples were located just before the diffuser, behind the radiance fiber and 5 mm from the cylindrical diffuser opposite side as the radiance fiber. The experiment is divided into two parts: the heating phase and the cooling phase. Both of them had used a different light source and detector.

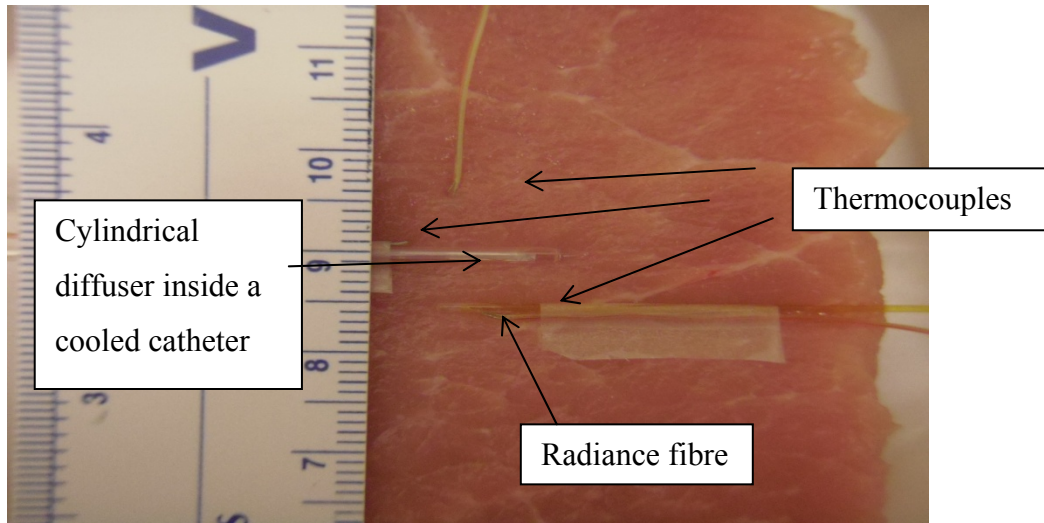


Figure 3.2.1: Experimental set-up. Fibre and thermocouple orientation, looking down at the bottom slab before heating.

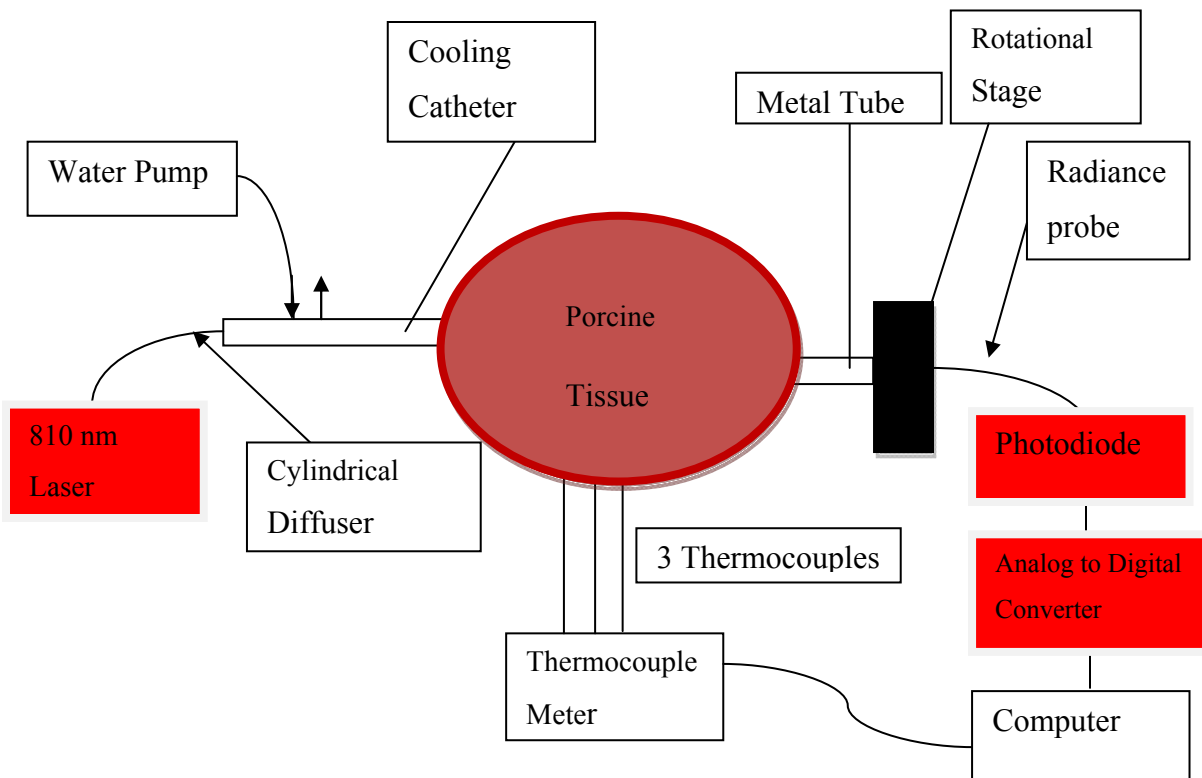


Figure 3.2.2: Schematic of the experimental set-up during the heating phase.

Heating Phase

Figure 3.2.2 shows the experimental set-up during the heating phase. A 1 cm long cylindrically diffusing fibre (Visualase, Visualase Inc., Texas, USA) with a core diameter of 400 μm was placed in a cooling catheter and connected to an 810 nm laser (Diomed-60, Diomed Ltd., Cambridge, UK). The laser is based on a gallium aluminum arsenide semiconductor diode light source. It outputs a maximum of 60 watts at 810 nm. The laser is coupled to an optical fibre using a SMA 905 connector. The power was set to 10 watts continuous wave during heating. 10 watts was chosen to provide strong heating. A high power was used because the cooling of the catheter would cool the tissue and would therefore increase heating time. A higher power was not used to prevent the risk of damaging the fibre. Figure 3.2.3 shows the cylindrical fibre inside a catheter where the water flows inside the catheter through the same inner tubing as the fibre and flows out through the outer tubing.

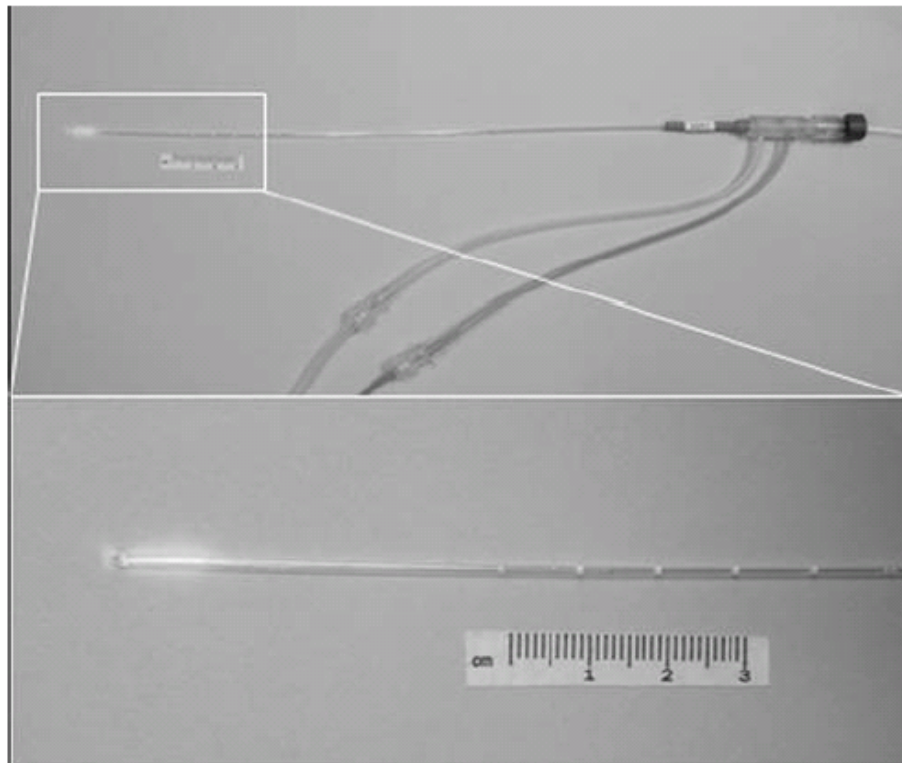


Figure 3.2.3: Picture of the cylindrical fiber inside the catheter (from Visualase Inc.). Picture from Schwartz *et al* 2011.

For detection, a radiance fibre (Fiberoptic Systems Inc., California, USA) with a core diameter of 600 μm was placed 5 mm away from the center of the diffuser and used as a

detector. It was aligned facing the cylindrical diffuser using a manual rotational stage (RSP1C/M, Thorlabs, New Jersey, USA). During heating, the radiance fibre was attached to an amplifying photodiode (PDA36A, Thorlabs, New Jersey, USA). The amplification was tuned manually to have a desired starting voltage. The maximum voltage from the diode is 10 volts. Based on preliminary experiments the radiance signal increased with heating time, the desired starting voltage was ~5 volts to allow the signal to increase without saturating and have a good signal-to-noise ratio. The PDA36A photodiode was chosen to detect the laser output at 810 nm light. Figure 3.2.4 shows spectral response of the photodiode. It contains a 3.6 x 3.6 mm detector and a 10 dB amplifier with 8 steps. The peak responsivity is at ~980 nm, the responsivity at 810 nm is ~87% of the maximum response.

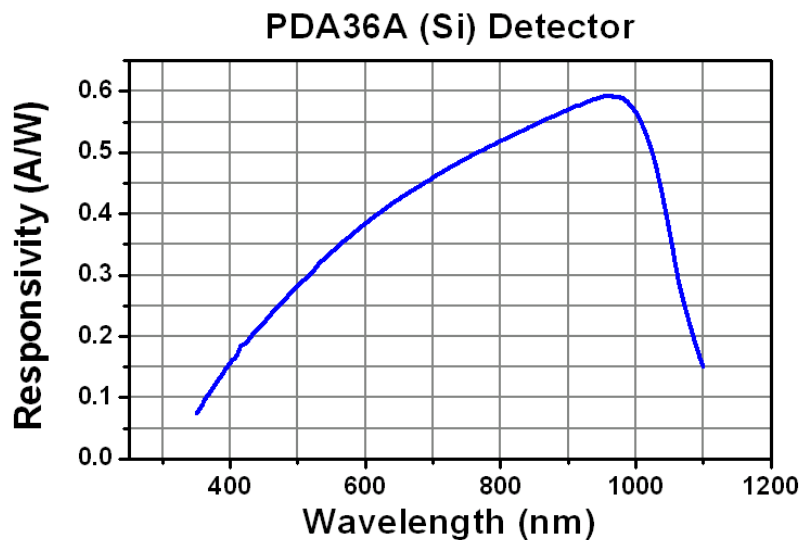


Figure 3.2.4: PDA36A photodiode spectral response (http://www.thorlabs.com/images/TabImages/PDA36A_response_large.gif).

Since the photodiode outputs a voltage it was then connected to an analog-to-digital converter (USB-1208LS, MCCDAQ, Massachusetts, USA) which was then read by a computer. Type K thermocouples attached to a datalogging thermometer (HH306A, Omega Engineering Inc., Connecticut, USA) were used to measure temperature at the heating fibre just before the cylindrical diffuser, behind the radiance fibre and 5 mm to the heating fibre but on the opposite side as the radiance fibre. A weight (rubber stopper) of ~150 grams and 6.5 cm in diameter was placed on top of the top slab to couple together the two slabs of tissue. Two heating protocols were used:

- i) 1 cm thick tissue was heated for approximately ~41 minutes.
- ii) 2 cm thick tissue was heated until a temperature of ~66 °C was achieved.

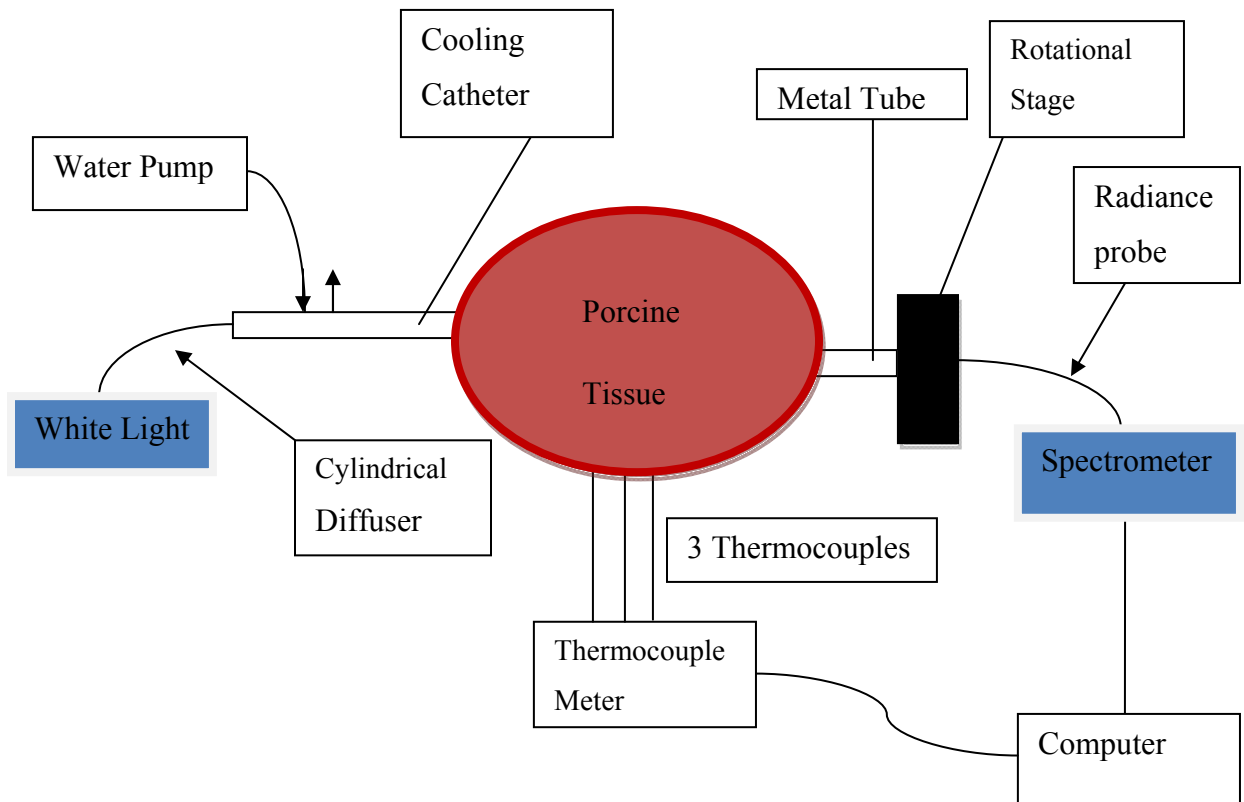


Figure 3.2.5: Schematic of the experimental set-up during the cooling phase.

Cooling Phase

Figure 3.2.5 shows the experimental set-up during the cooling phase with a different light source and detector than during the heating phase. Once heating was complete, the cylindrically diffusing fibre was disconnected from the laser and attached to a non-heating white light source (HL-2000). The radiance fibre was disconnected from the photodiode and attached to a spectrometer (USB4000, lens installed, electric dark correction). Spectra were acquired as the tissue was cooling.

For each experiment different integration times and averages were used due to the variable optical properties from tissue sample to tissue sample. Based on preliminary experiments the optical signal appeared to be stronger after heating than before heating. The integration time was varied (between 100 - 200 ms) to acquire a strong signal but not strong enough to saturate. The number of spectra averaged varied between 5 and 10 spectra with a total acquisition time for one spectrum of ~1 second.

3.3 Theoretical Radiance Calculations

Theoretical radiance calculations were performed to help explain the changes found between the heated and cooled spectrum in *ex vivo* tissue. Radiance was calculated at a distance of 5 mm from a spherical diffuser in coagulated tissue using the code by Liemert and Kienle (2011) which is based on an analytical solution to the radiative transfer equation for radiance. Due to the unavailability of the optical properties of porcine muscle in the NIR region, the optical properties were estimated based on bovine muscle and human muscle (Cheong *et al*, 1995, Kienle *et al*, 1996, Simpson *et al*, 1998). The absorption coefficient in cooled tissue was estimated to be 0.4 cm^{-1} with a water content of 70%. It was assumed that the optical properties are constant from 700 – 1000 nm based on the spectral optical absorption of human muscle (Simpson *et al*, 1998). The reduced scattering in muscle varies from 1.2 cm^{-1} to 8 cm^{-1} (Cheong *et al*, 1995, Simpson *et al*, 1998), for the simulations it was estimated the native reduced scattering was 4 cm^{-1} at 700 nm. These set of optical properties are similar to those of prostate (Svensson *et al*, 2007) in the NIR as seen in table 3.2.1. Furthermore, it was assumed that the reduced scattering increases 2 fold at 700 nm due to coagulation. The spectral reduced scattering coefficient was interpolated using equation 2.2. Figure 3.3.1 shows the estimated absorption coefficient and scattering coefficient in heated and cooled coagulated tissue that were inputted into the theoretical radiance model. The spectral values are between 700 and 1000 nm with 1 nm intervals. Three cases described below were simulated to help explain possible changes between the spectra acquired in heated tissue and in cooled tissue:

Case #1: Temperature-dependent optical absorption of water changes only with an increased temperature of 15°C .

Case #2: Temperature-dependent optical absorption of water changes with an increased temperature of 15°C and water concentration of water was reduced by 10% in cooled tissue.

Case #3: Temperature-dependent optical absorption of water changes with an increased temperature of 15°C and the reduced scattering coefficient was reduced by 10% in cooled tissue.

In each case the base absorption coefficient was 0.4 cm^{-1} . The absorption coefficient in heated tissue was found by increasing the base absorption coefficient with the temperature-dependent change in water absorption of 15°C. The increase absorption due to the temperature-dependence of water was scaled by 70%, the water content. In case #2, the absorption coefficient in cooled tissue was found by the decreasing the base coefficient by 10% of the water content (70%). Therefore, the decrease was 7% of the actual water absorption. The water absorption values and the temperature-dependent water absorption values were used from Hollis (2002) and Matcher *et al*, (1994) in figure 2.1.2.

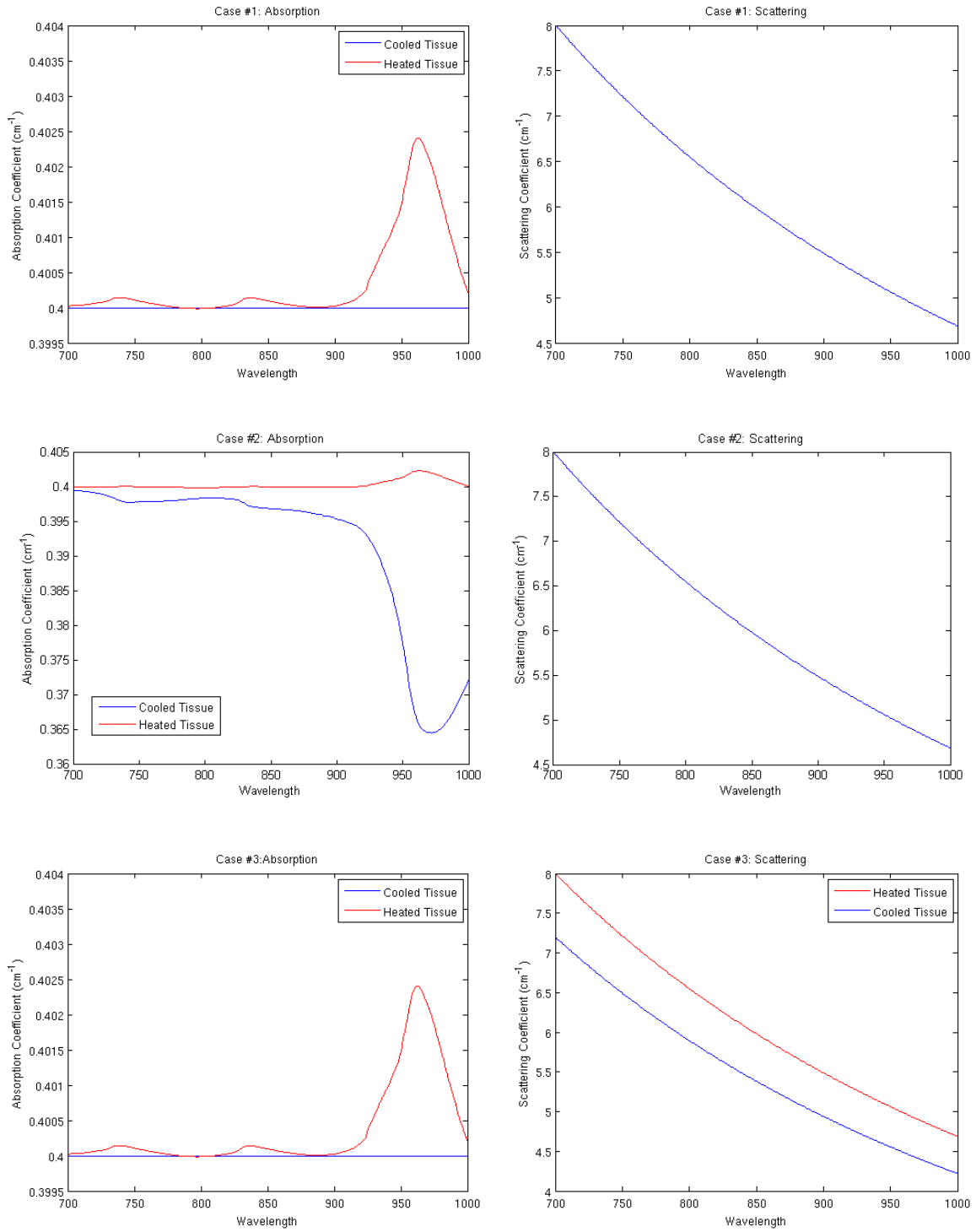


Figure 3.3.1: Optical properties in heated and cooled tissue for three different cases.

3.4 Data Analysis

To determine changes in the spectrum with temperature, the data is processed similar to an absorbance measurement using the following equation:

$$C = -\ln\left(\frac{I}{I_o}\right), \quad (3.2)$$

where I_o is the spectrum acquired at room temperature (either in water or air), I is the heated spectrum and C is the change between the two spectra. A ratio is used because changes in the spectrum can be better visualized. A natural log of the ratio is performed such that C is proportional to the change in absorption because by convention the attenuation of light in an absorbing medium and in tissue is described as an exponential decay. It is important to note that the system is not calibrated and equation 3.2 will not yield the actual absorption coefficient but rather will illustrate the spectral features of the detected chromophores.

For the first experiment using water, I and I_o in equation 3.2 were normalized to 700 nm, which is approximately the peak intensity in the acquired spectrum. The data were normalized because small movements in the fibres cause the intensity of the signal to change. By normalizing the spectrum, this change due to fibre movements is minimized. A wavelength of 700 nm was chosen for normalization because water exhibits very small changes in absorption due to temperature (discussed later) in comparison to temperature-dependent peaks which are located at approximately 739 nm, 837 nm and 962 nm. In addition, the relative absorption of water at 700 nm is low. The radiance system is not calibrated to give absolute radiance measurements but it does indicate how the radiance measurements change with a change in absorption

For the cases when I_o was the spectrum in water at room temperature or that of tissue that was cooled, the spectra were further processed in Matlab. In each spectrum, each point as well as 20 points to the left and 20 points to the right were averaged via boxcar filter to reduce noise and help locate spectral features.

4 Results and Discussion

4.1 Experiment #1: Water

4.1.1 Detecting Optical Absorption of Water

Figure 4.1.1 shows the raw spectrum in water and air while the fibres were guided into a phantom container with a source-detector distance of 1 cm. The raw signal is a combination of the response of the light source, spectrometer and the optical delivery and detection fibres. As a result, it is difficult to visualize changes in the raw spectra due to water absorption. By processing the spectra as an absorption like measurement as shown in figure 4.1.2, $-\ln(I_{water}/I_{air})$, where I_{water} is the normalized spectrum in water (where absorption exists) and I_{air} is the normalized spectrum in air (assuming no absorption), the changes due to the absorption of water at different wavelengths can be better visualized. The detected spectrum in water has a higher signal possibly due to a lower mismatch in the indices of refraction between water and silica.

It needs to be emphasized that the radiance system is not calibrated to give an absolute absorption measurement because the system does not use a collimated light source or detector. More specifically, the detection fibre has a curved surface with a cap which can cause light to refract into the fibre's acceptance cone and increase the signal. Nevertheless, the measurements and the method of analysis chosen do give a non-absolute relative change in the detected absorption over the spectrum. Water absorption features are observed at 744 nm (weak), 840 nm (weak) and 973 nm (strong).

An important remark regarding the ability of this radiance approach to detect water absorption is that the detected peak is not at 973 nm but at 964 nm when comparing with Matcher *et al* (1994). Matcher *et al* had detected a broader absorption peak at 973 nm compared to that observed in this radiance study. It is not entirely known why the experimental data detects lower full width half maximum at this location. One possibility is that a different type of detector was used in their study, Matcher *et al* (1994) do not specify the type of detector used in their study. A Gallium Arsenide (GaAs) detector is required to measure light past 1,000 nm wavelengths because the efficiency of silicon detectors decreases significantly.

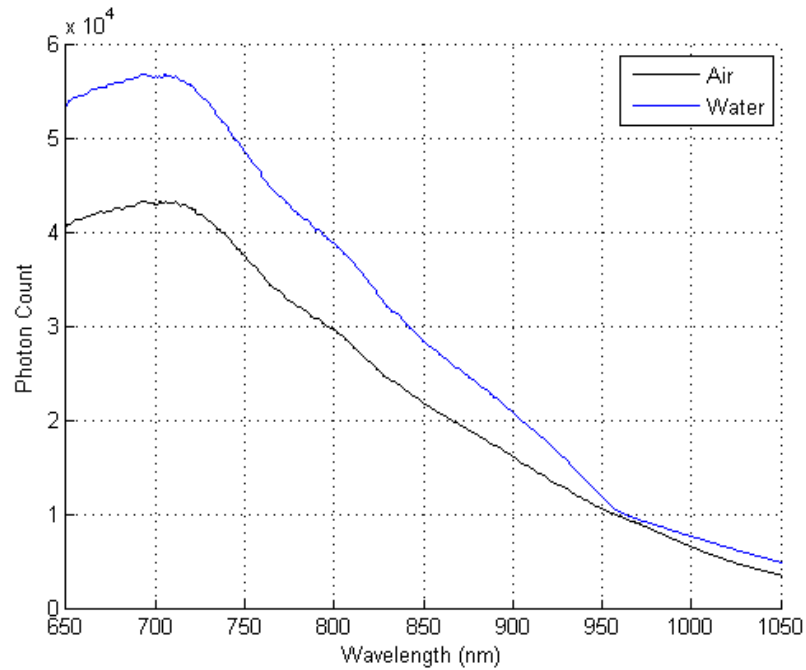


Figure 4.1.1: Raw optical spectra in air (black) and in water (blue).

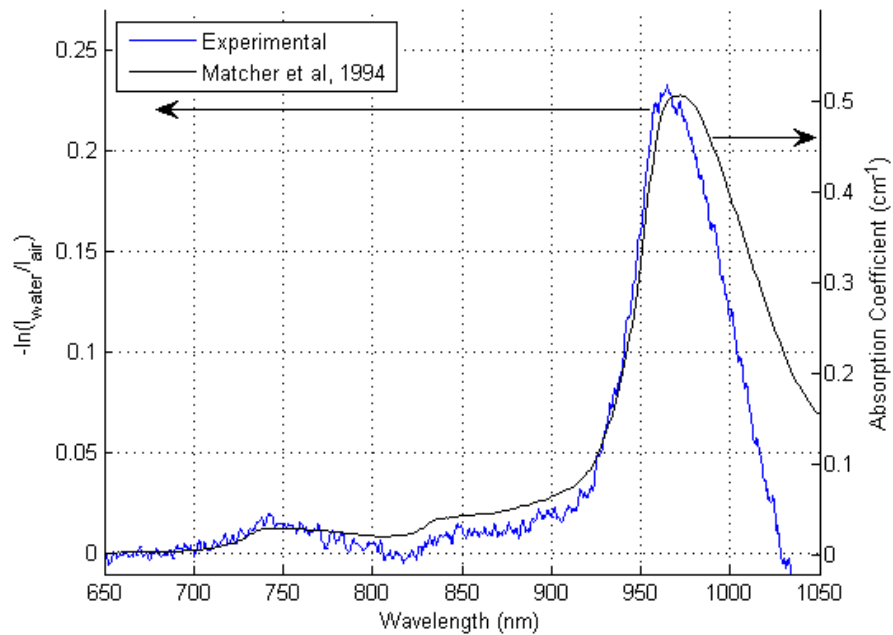


Figure 4.1.2: Ratio of optical radiance signals from air-to-water as an absorption measurement (left axis). The absorption coefficient of water absorption from Matcher *et al* (1994) is also presented (right axis). Experimental data normalized to 700 nm.

4.1.2 Temperature-Dependent Changes in Water Absorption

The radiance measurements were used to detect the temperature-dependent changes in optical absorption of water. Figure 4.1.3 illustrates the change in optical absorption in water with temperature. A clear trend can be observed in the change in absorption at ~ 960 nm. In the spectra measured in this study, there is no measurable shift in the absorption peak, while Chung *et al* (2010) show the 973 nm band shifting to lower wavelengths (called a blue-shift) with increased temperature. This is most likely due to the radiance measurements showing peak water absorption at 963 nm and not at 973 nm.

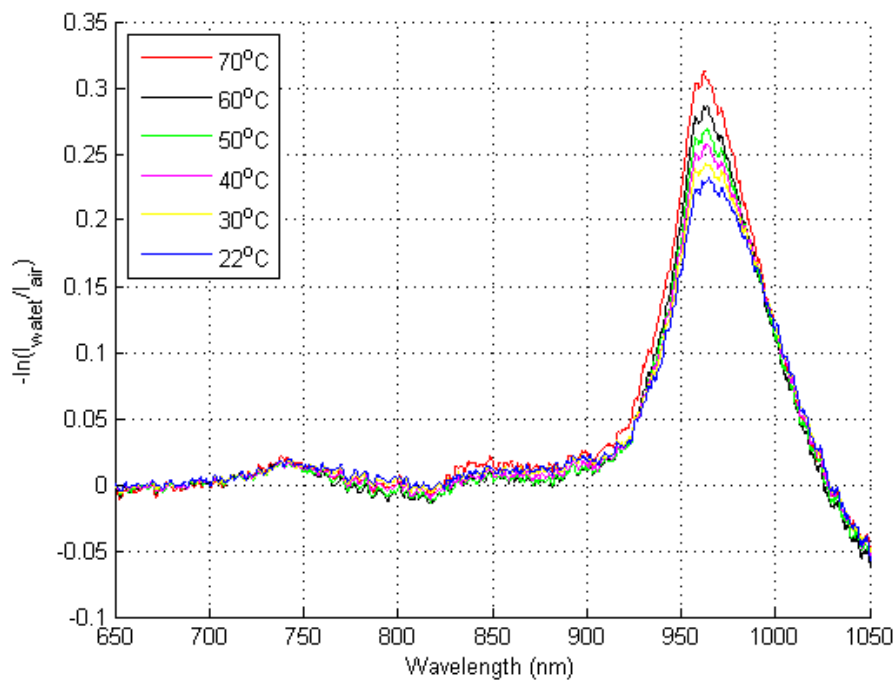


Figure 4.1.3: Spectral radiance ratio as a function of temperature from 22°C - 70°C. Experimental data normalized to 700 nm.

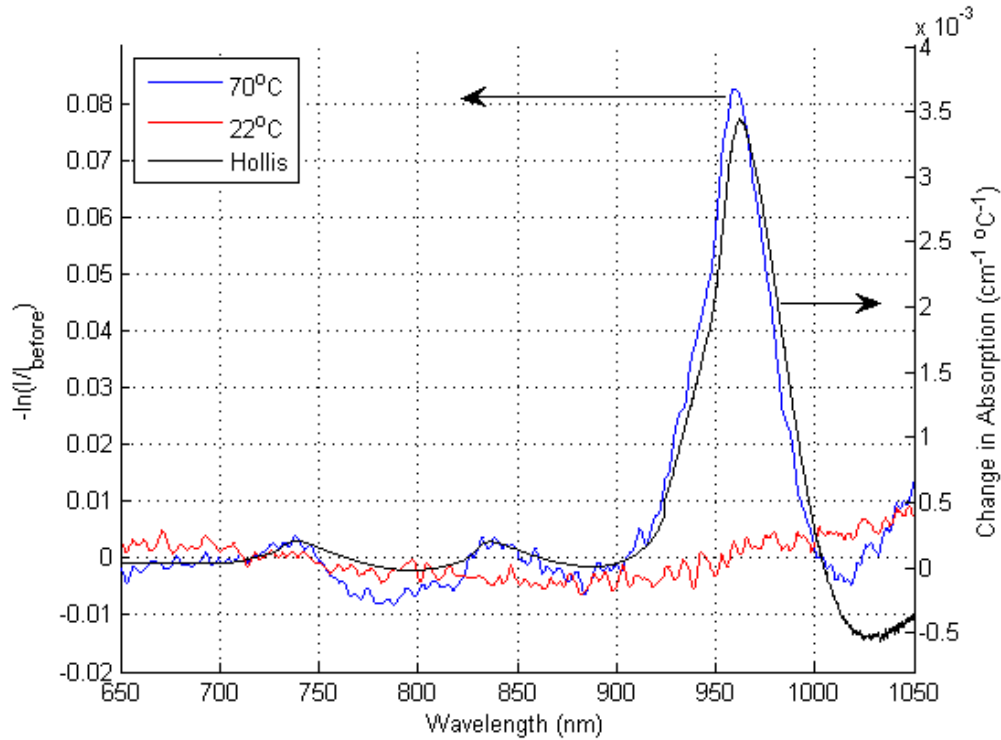


Figure 4.1.4: Spectral radiance ratio in water (I) relative to water at room temperature before heating (I_{before}) (left axis). The temperature dependent change in the optical absorption coefficient of water (from Hollis 2002) is presented for comparison (right axis). Experimental data normalized to 700 nm.

Furthermore, temperature-dependent absorption peaks at 738 nm and 836 nm are also detected. These peaks can be observed when processing the data such that I_o in equation 3.2 is the spectrum acquired in water at room temperature. Figure 4.1.4 shows the changes in the absorption spectrum of water with the maximum change at 70°C and after the water had cooled relative to the spectrum acquired at room temperature before heating. The wavelength with largest changes found in the radiance at 70°C was at 960 nm compared with Hollis' data at 962 nm. The changes in absorption after heating do not go back to zero most likely due to fibre movement and misalignment during heating. One possible reason for such a shift is that the spherical source and/or radiance detector could have moved in such a way where the fibres are no longer facing each other directly or the distance between the two fibres could change. Another source of error can be due to bubble formation due to heat. Although preheating the water in a kettle reduces bubble formation it is not eliminated during heating. Using a cylindrical diffuser

with the same heating protocol such a problem would be reduced. If the radiance fibre moves to face the upper or lower portion of the cylindrical fibre the detecting fibre would still observe a cylindrically emitting light source.

4.1.3 Temperature-Dependent Changes in the Acceptance Angle

Full 360° radiance data was acquired in air, room-temperature water and heated water to investigate a possible change in the acceptance cone of the radiance fibre. Figure 4.1.5 shows the relative change in intensity as a function of angle away from the light source in air and room temperature water. The Full Width Half Maximum (FWHM) is a measure of the angle width at which over 50% of the light is detected. Such a measure is similar to the numerical aperture which is related to a fibre's acceptance cone. Figure 4.1.6 shows the FWHM over the acquired spectrum. The numerical aperture of the fibre provided by the manufacturer is 0.22 (The manufacturer does not specify the wavelength); this gives a FWHM of 25.42° in air. This differs from the experimental FWHM, which is 23.01° at 810 nm, by a percent difference of 9.5%. Manufacturers typically provide the NA for plain cut fibres, but since these are fibres cleaved at an angle and the surface of the detector is curved instead of being flat and therefore the NA of these fibres will differ. The acceptance angle in air is greater than in water because a greater mismatch in the index of refraction exists between the fibre and the medium causing light to refract more and be detected. This effect works in two ways: 1) collection angle increases due to light refraction and 2) higher Fresnel reflections occur due to higher mismatch in the indices of refraction. A higher acceptance angle in the radiance probe can be observed in heated water because the index of refraction of water decreases and in silica increases with temperature causing an increase in the mismatch in the index of refraction between the optical fibre and the medium. The difference in the FWHM of the radiance probe before heating (in water) and after cooling (in water) is 13.99° and 13.56° respectively a difference of 0.43°. This difference may be due to fibre movement or due to angular resolution. The FWHM angle of the detected signal was interpolated based on the two closest points which were 1° apart, this interpolation introduces additional approximation error. The FWHM of the radiance probe in heated water was 15.47° and differs with the detected FWHM in room temperature water by at least 1.48°. These differences are small in the context of the experiments conducted because the light source is not large and the majority of light detected is directly from the light source at the same height. If using a large light source or a cylindrical light source the changes in the FWHM due to heated

water may affect the intensity detected. As the acceptance cone changes light further along a cylindrical diffuser would be detected. A similar scenario is presented in a turbid medium where light detected at a particular point is from multiple directions caused by scattering.

Other features in heated water found in Figure 4.1.6 are: a slight increase in FWHM at ~ 700 nm relative to wavelengths in the range of 600 – 820 nm and a peak 960 nm. Also a small increase in intensity is observed at $\sim 125^\circ$ from the light source. This is likely due to the radiance fibre not being coated on the hypotenuse thus allowing some light to enter the fibre from the back at those angles.

Using the experimental FWHM acceptance in water at 810 nm the NA is 0.1620 using equation 2.3. Using this NA and assuming core index of refraction as 1.46, the index of refraction of the cladding is 1.4510 using equation 2.4. Using the temperature-dependent changes for the index of refraction of water as $-95 \times 10^{-6}/^\circ\text{C}$ and for silica as $12.8 \times 10^{-6}/^\circ\text{C}$ from figure 2.2.1, table 4.1.1 shows how the acceptance angle changes with temperature. A change in the temperature of silica of both core and cladding decreases the acceptance angle of the fibre, while a change in the index of water increases the acceptance angle. The table does not agree completely with the experimental data but indicates which of the parameters affect the acceptance angle of the fibre the most. Based on these theoretical calculations, the changes in the indices of refraction of water and the core of the fibre have the most effect on the acceptance angle variation with temperature.

Fresnel reflections due to changes in the indices of refraction of water and silica contribute a small change in the detected optical intensity. For a collimated light beam the percent difference in reflection at a water/silica interface between heated and non-heated water conditions is 0.0878%, meaning there is less than 1% increase in reflection due to heating. For angles 0° - 60° , which are angles at which light is detected, the overall percent difference in reflections is 4.7592%. If one were to account for the acceptance angle of the fibre, the percent difference would be even smaller. However, to quantify this and compare with the experimental data is difficult because the data was normalized due to the potential movement of the fibres.

Using this data to predict how the index of refraction would affect the optical signal in a turbid medium such as tissue is difficult. Grabtchak *et al* (2011) have shown that the FWHM is much larger in a turbid medium. In addition, the index of refraction of tissue is 1.4 not 1.33 like

water and the temperature-dependent changes in the index of refraction of tissue have not been thoroughly investigated.

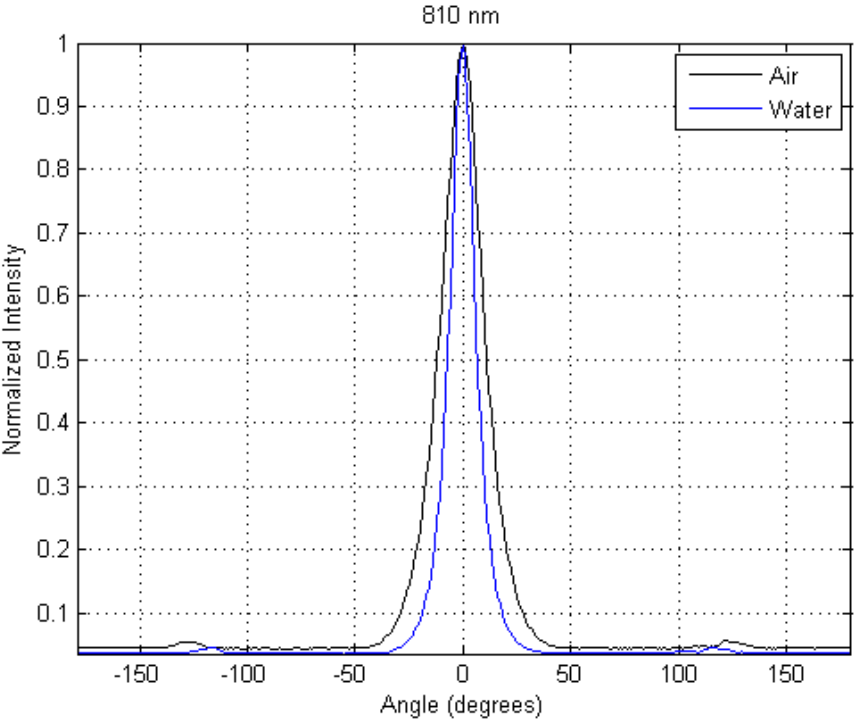


Figure 4.1.5: Relative Radiance as a function of angle away from the light source at 810 nm.

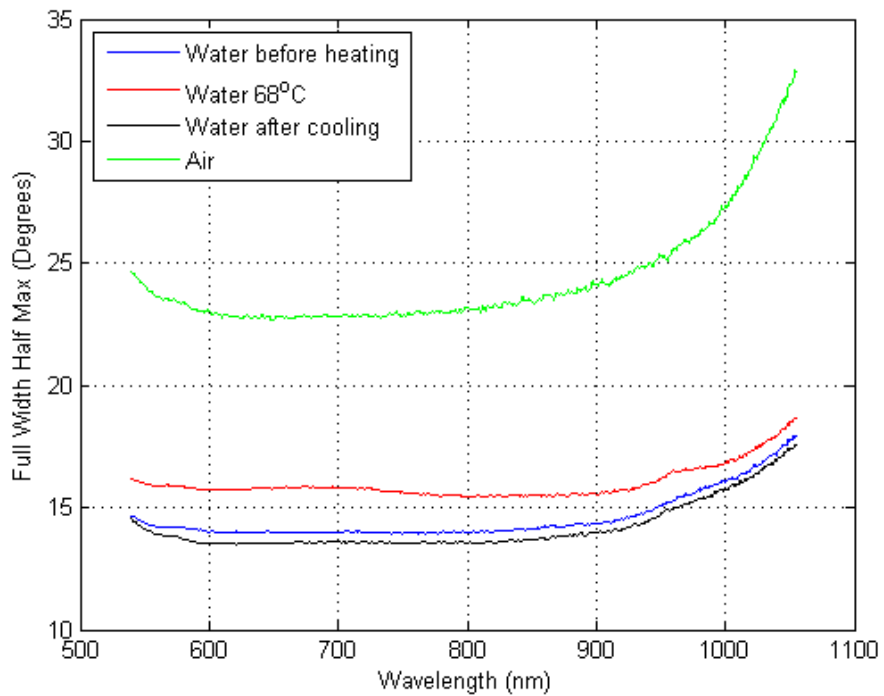


Figure 4.1.6: Full Width Half Maximum (FWHM) in water before heating, heated water at 68°C, cooled water, and air.

Table 4.1.1: Estimated acceptance angles of our plane cut fiber materials and water with 50°C increase in temperature.

Temperature Changing Parameter	Full Width Acceptance Angle
No change (Room temperature)	13.99
Water only	14.0308
Water and core of the fibre	14.5253
Water, core and cladding of fibre	14.0339
Core and cladding of the fibre	13.9835

4.2 Experiment #2: *Ex Vivo* Tissue

The overall goal of using radiance measurements during thermal therapy is to monitor the extent of thermal damage. *Ex vivo* tissue heating experiments were conducted to simulate a clinical setting whereby biological tissue is used. These experiments helped determine the possibility of a change in the optical signal during the cooling of the tissue.

4.2.1 Dynamic Change in the Radiance Signal with Heating

Figure 4.2.1 shows the coagulated tissue due to laser heating which is represented as the white region compared to native tissue which is a pink colour. The coagulated tissue is not sharply demarcated from the native tissue but rather more diffuse. This suggests a more gradual temperature gradient during heating. Figures 4.2.2 and 4.2.3 shows the radiance signal changes with heating time due to coagulation, however, the change in the radiance differ from Chin's *et al* (2004). Chin *et al* (2004) had observed a decrease in radiance while the radiance found during heating of porcine muscle had increased in this study. The difference in the observed detected radiance can be due to the diffuse-like coagulation seen in our experiments causing the optical signal to behave differently. The diffuse coagulation may be caused by slow heating due to low absorption.

The laser is turned on for a short period of time (~10 seconds) to set-up the correct amplification such that the radiance signal is strong but not saturating. Consequently, a spike in temperature can be seen just before heating. This part of the radiance signal was not plotted in the figure to prevent confusing the reader and simply show that the radiance signal changes gradually with heating time. Also, the temperature measurements increase and decrease sharply at the beginning and end due to self heating of the thermocouples due to the laser turning on and off. Self heating is produced when the thermocouple absorbs the light energy and converts it to heat. As a result, the thermocouples overestimate the temperature. Temperature was lowest at the cylindrical fibre due to the cooling effect introduced by the flow of water in the catheter.

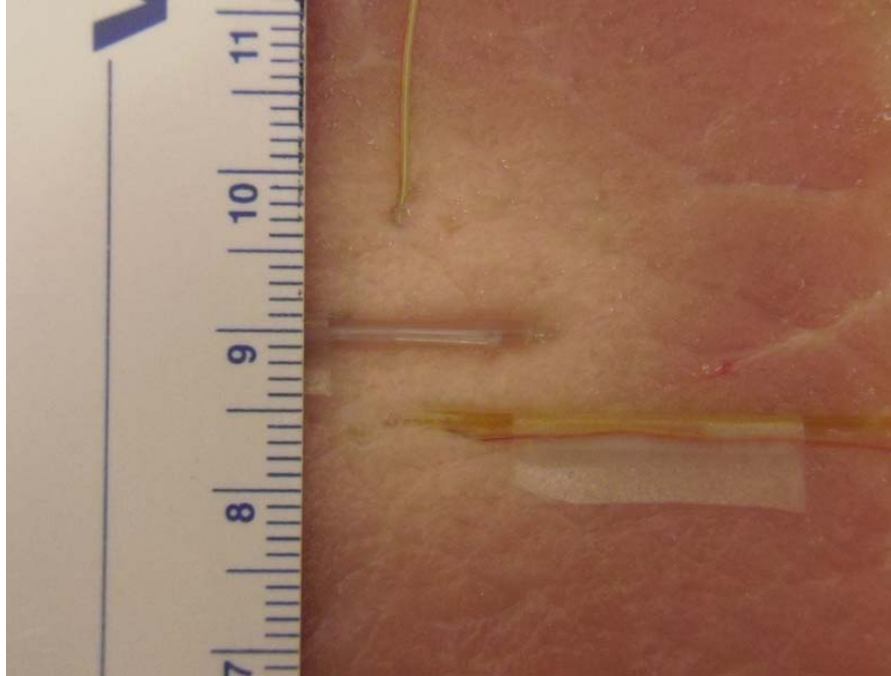


Figure 4.2.1: Bottom slab of porcine muscle after heating. Coagulated tissue shown as a white colour due to laser heating.

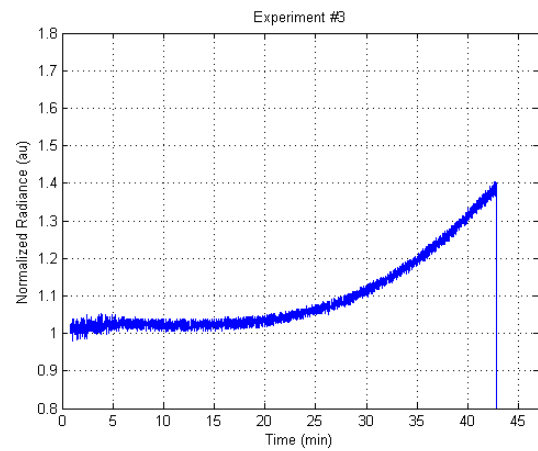
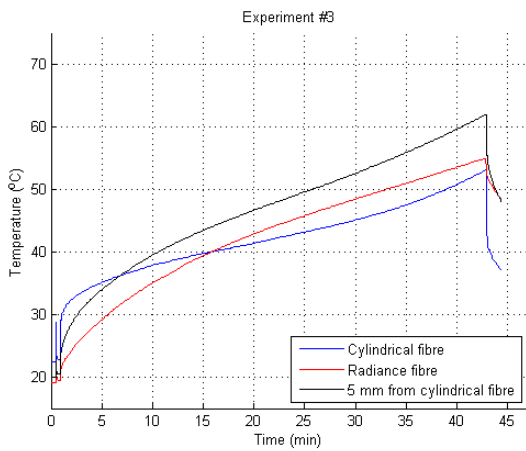
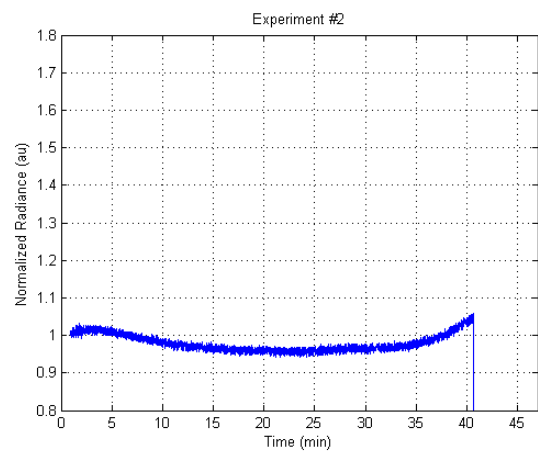
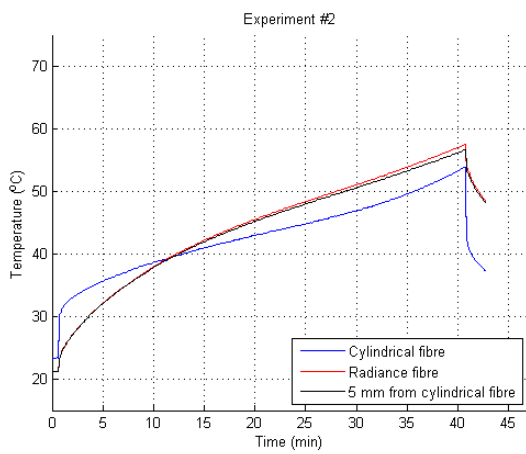
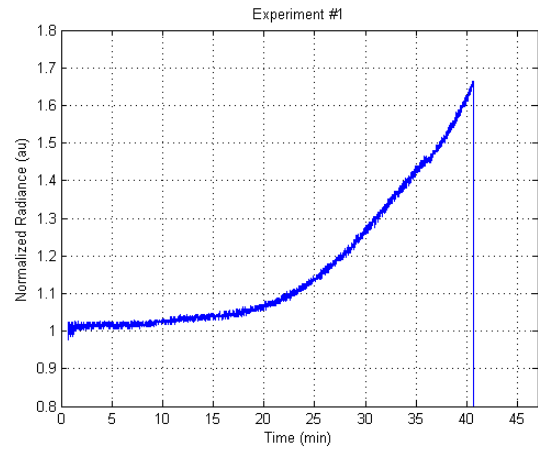
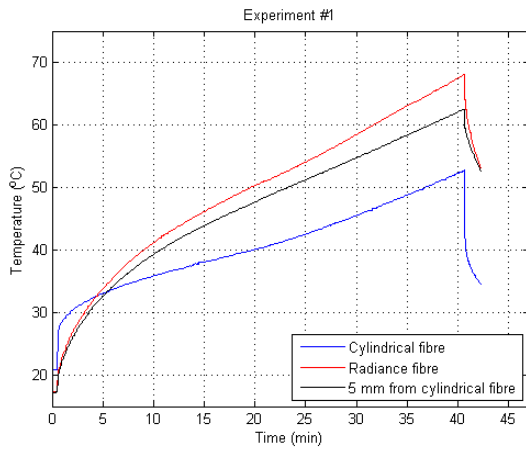


Figure 4.2.2: Temperature profile and normalized radiance signal with time starting with the first temperature measurement for experiments using heating protocol i).

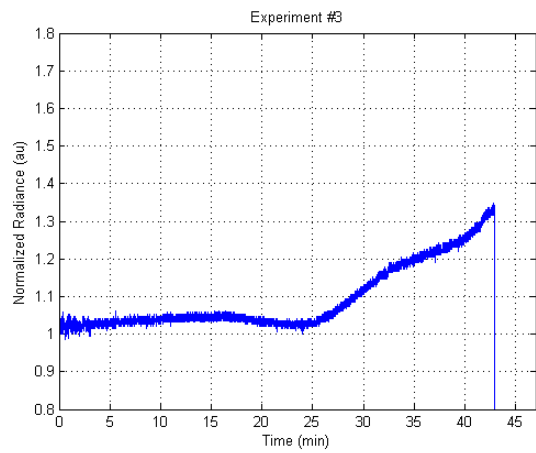
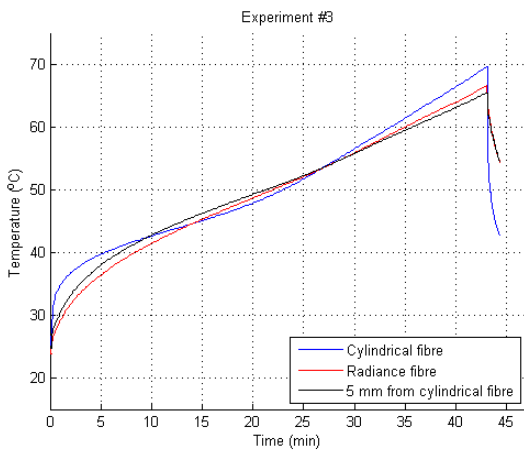
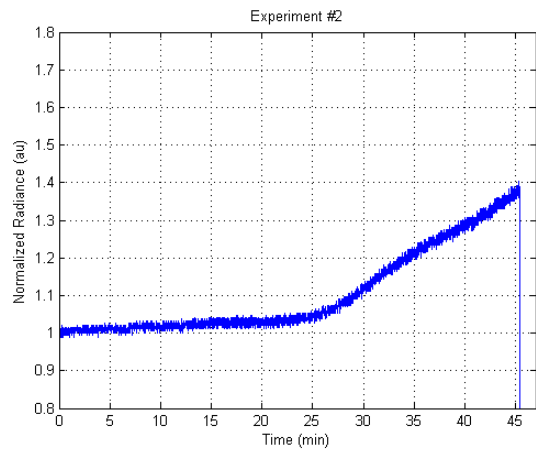
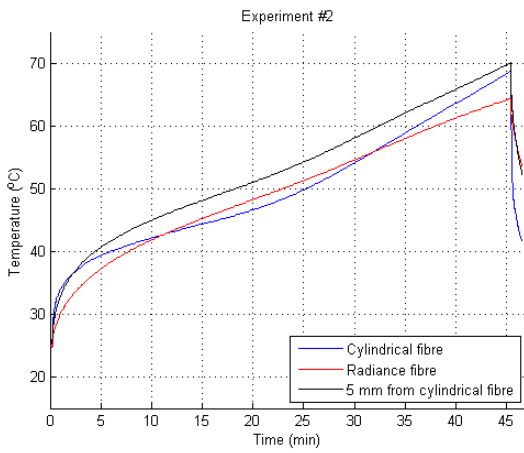
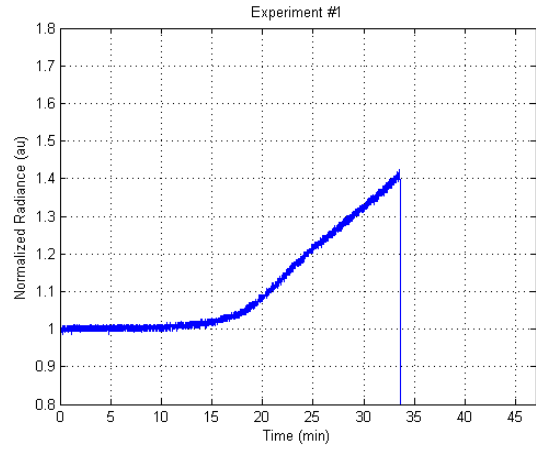
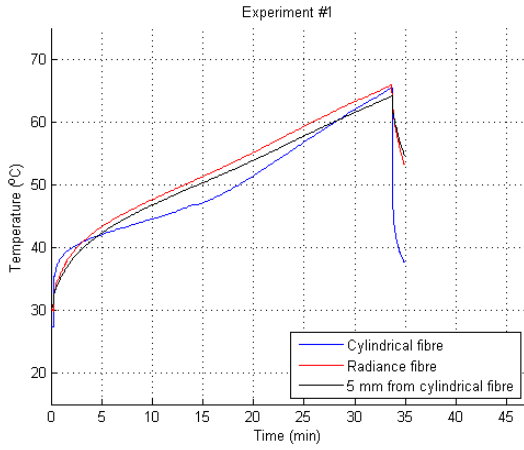


Figure 4.2.3: Temperature profile and normalized radiance signal with time starting with the first temperature measurement for experiments using heating protocol ii).

4.2.2 Comparing the Radiance of Heated Tissue with Cooled Tissue

Investigation in ex vivo tissue was undertaken to determine whether the radiance signal has changed due to a permanent effect due to thermal damage or if changes in the radiance signal are due to a reversible effect that does not represent thermal damage. Table 4.2.1 and table 4.2.2 show the maximum temperature, and temperature in the first and last spectra. The maximum temperature was achieved just prior to turning the laser off. The temperature of the tissue during the acquisition of the first spectrum was higher than all other acquired spectra, while the temperature in the last acquired spectrum was when the tissue had cooled most. This table can be used as a reference for comparing the changes in the spectra in figure 4.2.4. This figure shows a comparison between the first spectrum acquired (I_{heated}) with the last spectrum (I_{cooled}), which is the maximum difference in tissue temperature while spectra were acquired. Figure 4.2.4 shows important features, peaks in the detected radiance ratio located at approximately 739 nm, 837 nm and 960 nm. These spectral peaks coincide with the same peaks as the temperature-dependent changes of water absorption observed in our first study. Table 4.2.3 shows the location of the detected peaks where the 739 nm, 837 nm and 962 nm deviated most with temperature-dependent peaks of water to 4 nm, 6 nm and 2 nm, respectively. For each of these peaks the average and standard deviation is 739.9 ± 1.9 nm, 838.8 ± 3.4 nm and 962.0 ± 1 nm. The highest standard deviation was 3.4 nm at 838.8 nm due to two experiments whose peak deviated by 6 nm. Overall, the average recovered peak locations were accurate and significant compared to an optical resolution of ~ 2 nm. The exact locations are tabulated in table 4.2.3. Experiment #1 using heating protocol i) (heating for ~ 41 minutes) exhibits the largest changes in that set of experiments because the difference in temperature is greatest. Changes at 960 nm were larger in the experiments using heating protocol ii) (minimum temperature of $\sim 66^\circ\text{C}$ is achieved) than in heating protocol i) likely due to the fact that the first spectrum and the final cooled spectrum have a higher difference in temperature. With this radiance ratio method $-\ln(I_{heated}/I_{cooled})$, a positive value means the optical attenuation is higher in heated tissue (first spectrum, I_{heated}) than in cooled tissue (last spectrum, I_{cooled}). In experiments #2 and #3 using heating protocol ii), there is a shift in the detected signal change where there appears to be a baseline shift. The cause for this shift is likely due to the movement of the fibres. What the results suggest is that during the cooling of the tissue the distance between the fibres had increased. In addition to the temperature-dependent water absorption, a feature at ~ 775 nm is also observable in most

experiments. Temperature-dependence of another unidentified chromophore(s) could be occurring causing a higher signal to occur at higher temperatures. Overall both heating protocols yield temperature-dependent peaks of water absorption in all experiments.

Table 4.2.1: Temperature measurements for experiments using heating protocol i).

Experiment	Time (min)	Max Temperature Achieved (°C)			Temperature in the First Spectrum (°C)			Temperature in the Cooled Spectrum (°C)		
		Radiance Fibre	Cylindrical Diffuser	Opposite the Radiance Fibre	Radiance Fibre	Cylindrical Diffuser	Opposite the Radiance Fibre	Radiance Fibre	Cylindrical Diffuser	Opposite Side the Radiance Fibre
# 1	40.15	68.1	52.8	62.5	53.3	34.6	52.7	30.9	25.6	31.3
# 2	40.16	57.5	53.9	56.6	48.5	37.4	48.2	33.5	29.3	33.6
# 3	42.00	55.0	53.1	61.9	48.5	37.3	48.3	34.7	29.4	33.7

Table 4.2.2: Temperature measurements for experiments using heating protocol ii).

Experiment	Max Temperature Achieved (°C)			Temperature in the First Spectrum (°C)			Temperature in the Cooled Spectrum (°C)		
	Radiance Fibre	Cylindrical Diffuser	Opposite the Radiance Fibre	Radiance Fibre	Cylindrical Diffuser	Opposite the Radiance Fibre	Radiance Fibre	Cylindrical Diffuser	Opposite Side the Radiance Fibre
# 1	66.0	65.5	64.2	53.4	37.7	54.7	33.1	27.8	33.7
# 2	64.4	68.7	70.1	53.9	42.0	52.6	33.9	29.1	32.6
# 3	66.6	69.6	65.5	54.4	42.8	54.5	34.4	29.8	34.2

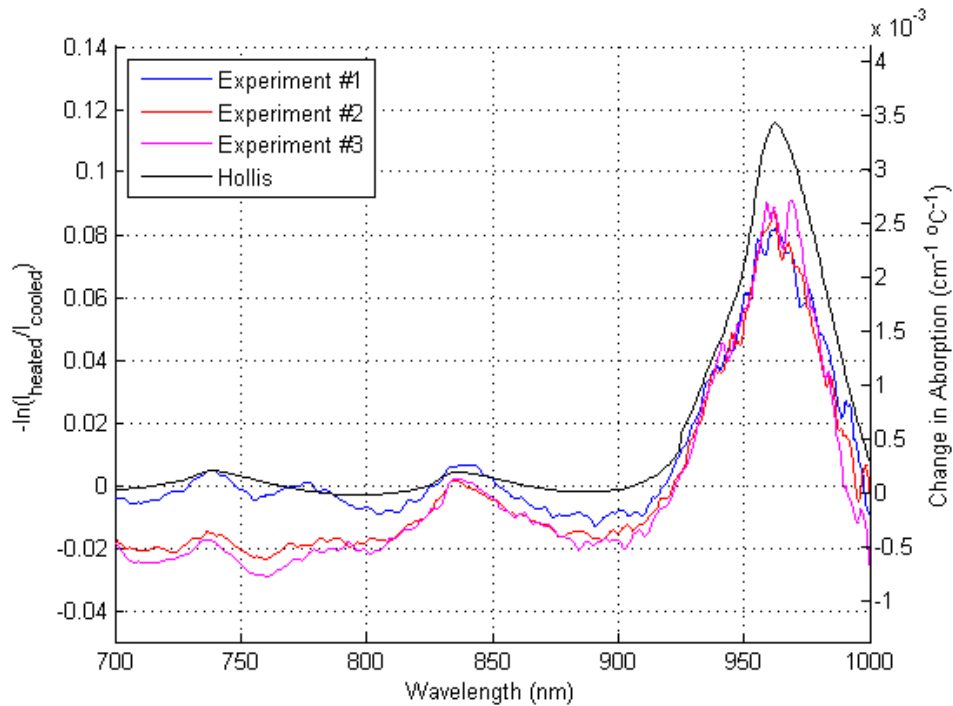
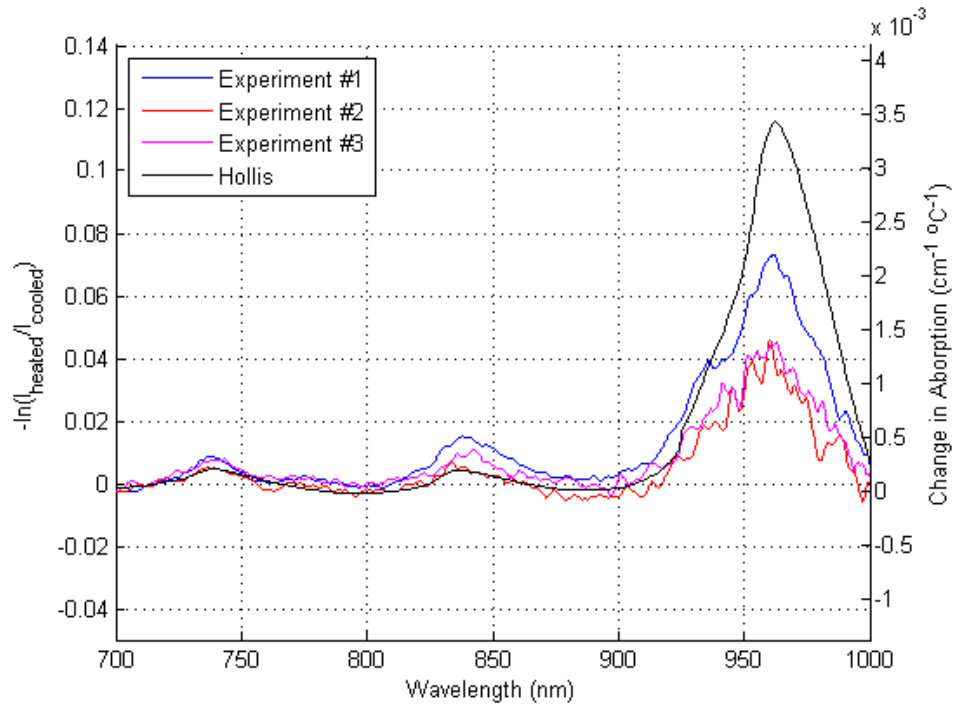


Figure 4.2.4: Spectral changes where I_{heated} is the first spectrum (heated tissue), I_{cooled} is the last spectrum (cooled tissue) on the left axis compared with Hollis' temperature-dependent change in water absorption of water on right axis. Top graph using experimental protocol i) and bottom graph using protocol ii).

Table 4.2.3: Location of the Temperature-Dependent Optical Absorption Peaks Measured in coagulated *ex vivo* porcine muscle.

Peak locations (Hollis, 2002)		739 nm	837 nm	962 nm
Heating Protocol i)	Experiment #1	739 nm	840 nm	962 nm
	Experiment #2	740 nm	834 nm	960 nm
	Experiment #3	743 nm	843 nm	963 nm
Heating Protocol ii)	Experiment #1	739 nm	843 nm	963 nm
	Experiment #2	737 nm	836 nm	962 nm
	Experiment #3	738 nm	837 nm	962 nm
Average		739.3 nm	838.8 nm	962.0 nm
Standard Deviation		1.9 nm	3.4 nm	1.0 nm

Although temperature-dependent changes due to water in the radiance signal exist, the next section will address the significance of these changes in the context of thermal therapy. Figures 4.2.5 and 4.2.6 show the raw radiance spectra obtained from the tissue: before heating, immediately after heating and after a cooling period which varied between approximately 18-25 minutes. These figures illustrate that the changes in heated tissue and cooled tissue are very small compared to the changes due to thermal damage (before heating and cooled tissue). Therefore, the changes found during the cooling phase are not significant in the context of monitoring thermal therapy.

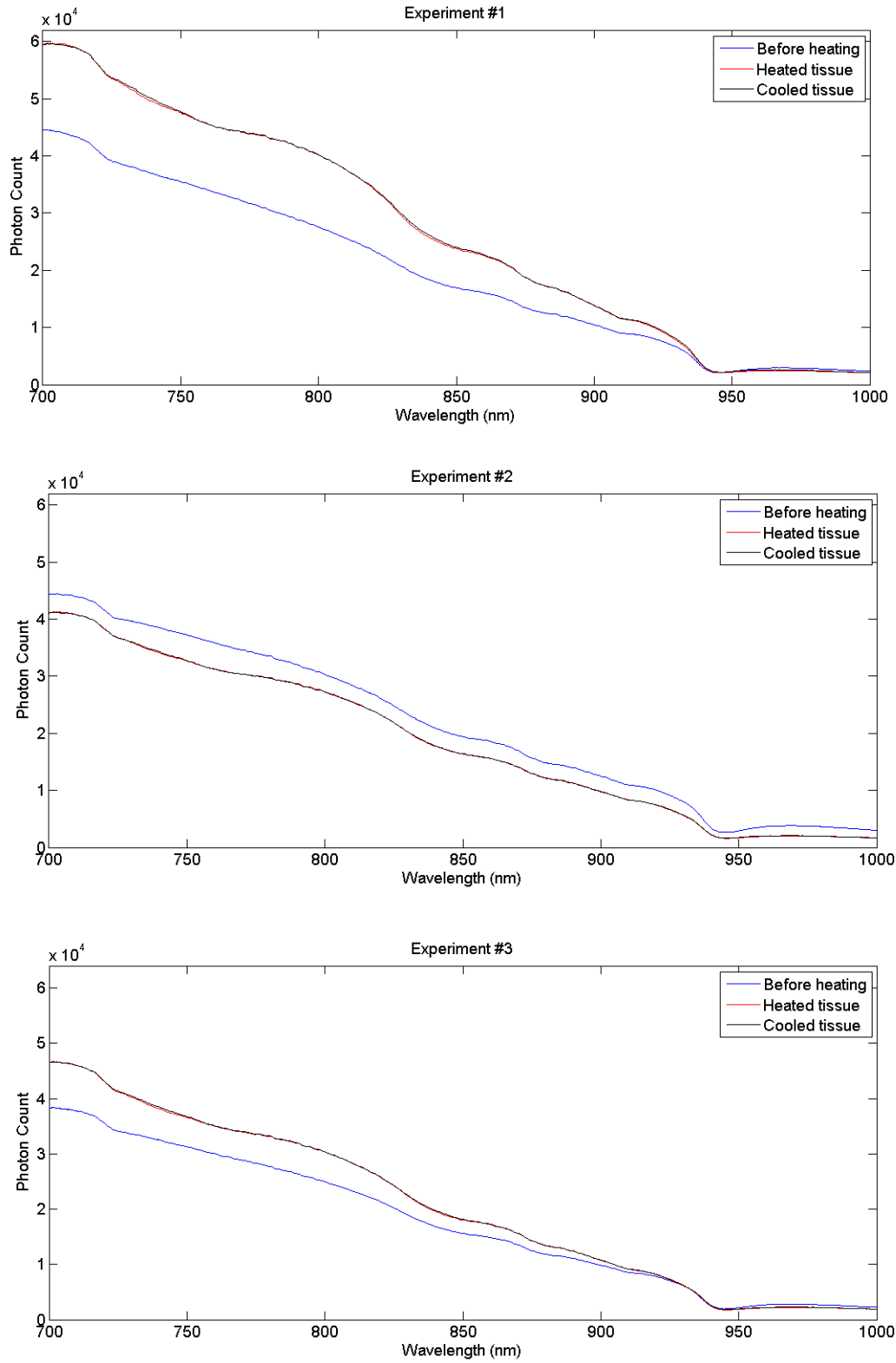


Figure 4.2.5: Raw radiance signals obtained in porcine muscle tissue before heating, immediately after heating and after cooling using heating protocol i).

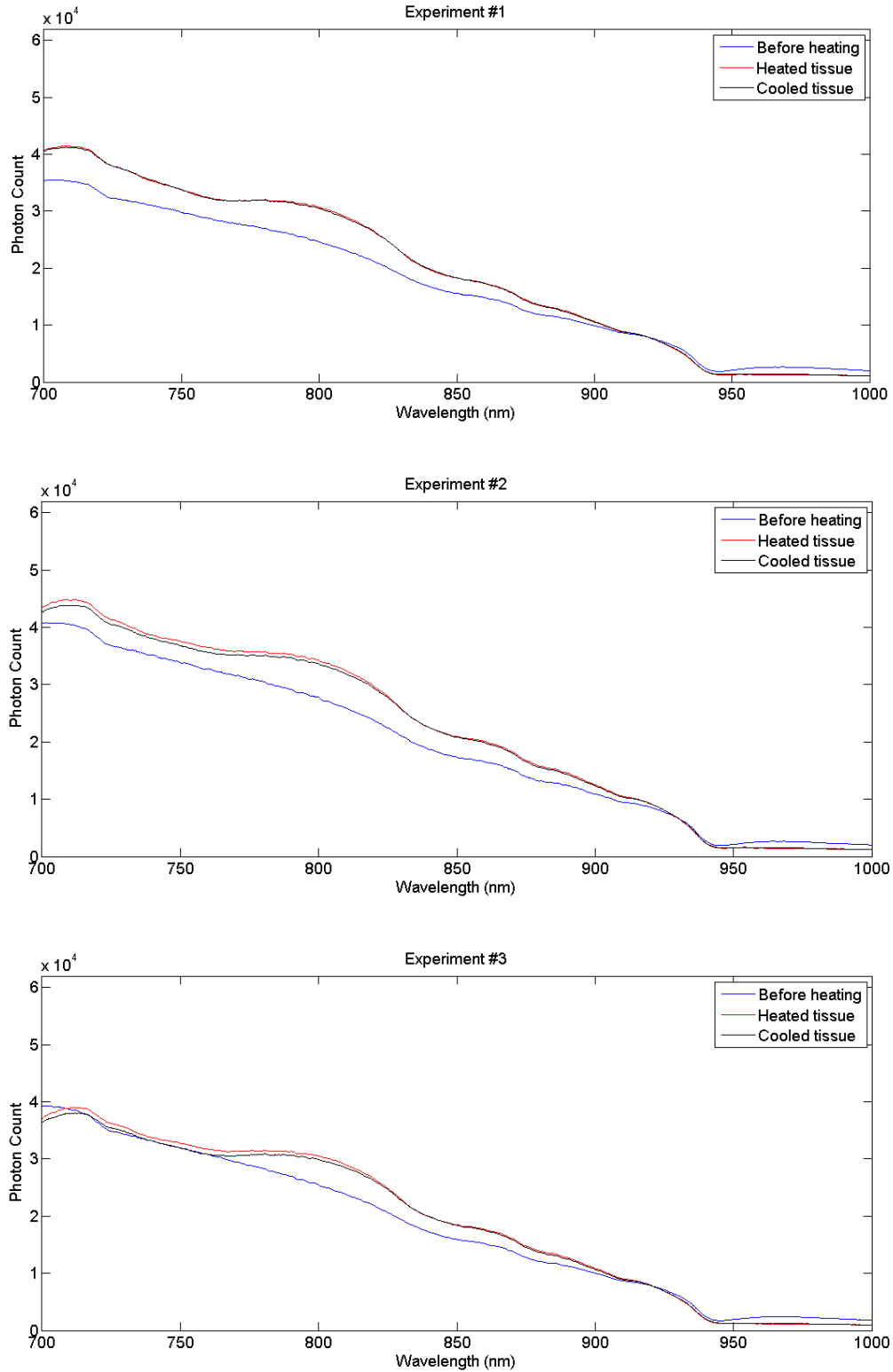


Figure 4.2.6: Raw radiance signals obtained in porcine muscle tissue before heating, immediately after heating and after cooling using heating protocol ii).

Furthermore, the changes in the spectra relative to the cooled spectra were plotted as a function of time. The purpose for presenting this is to prove that there were no abrupt changes but rather gradual changes in the spectra with time. Changes as viewed in Figure 4.2.7 are temperature-dependent most notably at 962 nm. As the temperature of the tissue decreased, the change at 962 nm (where the changes due to temperature are largest) also decreases. Weaker peaks at 739 nm and 837 nm are also visible.

To ensure that the changes in radiance are related to temperature, the peaks at 740 nm, 840 nm 960 nm were plotted as a function of time relative to 700 nm and compared with the change in temperature. Figure 4.2.8 illustrates that both the spectral changes, using equation 3.2, with time and temperature decay exponentially. This suggests that the changes in the spectrum are related to temperature. However, changes at 739 nm for experiments #2 and #3 were not visible. This is most likely due to the “shift” in the spectral change at those locations causing these peaks to appear too small to detect in amplitude relative to 700 nm.

Overall, the experimental results show that radiance measurements mostly represent permanent changes to thermal damage but small changes in the optical absorption of water with temperature can be detected in tissue.

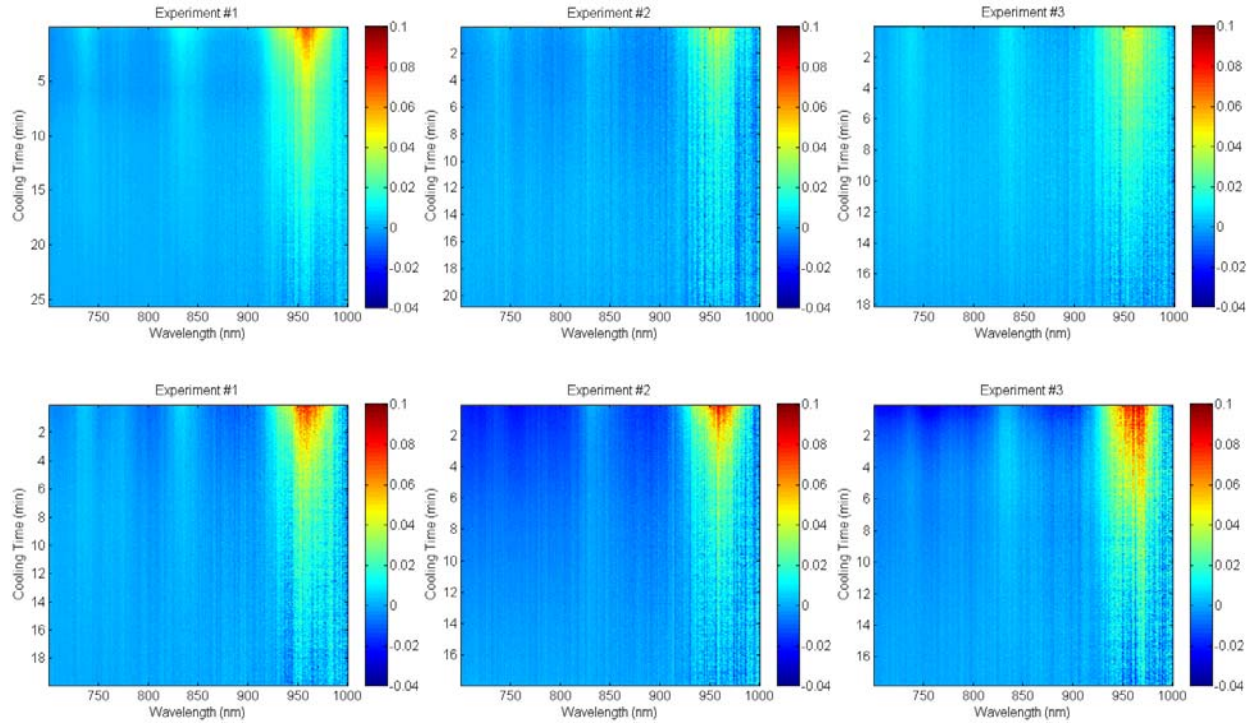


Figure 4.2.7: Changes in the optical radiance ratio spectrum with time. Colour represents the change $-\ln(I_{heated}/I_{cooled})$, where I_{heated} represents the heated spectrum at a particular time point and I_{cooled} is the last spectrum. Top experiment show results using experimental protocol i) and bottom experiments show results using experimental protocol ii).

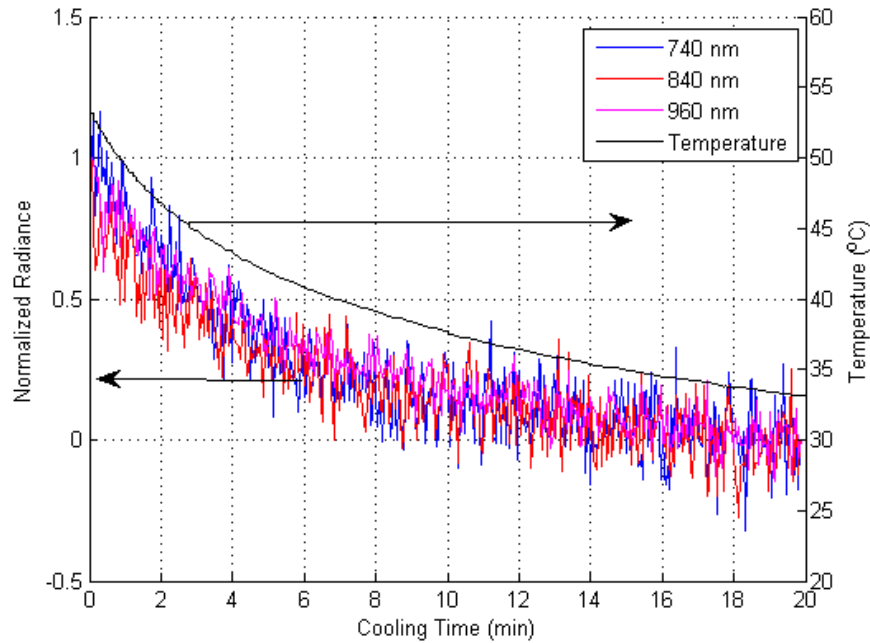


Figure 4.2.8: Change in the spectrum with time, $-\ln(I_{heated}/I_{cooled})$, at 740 nm, 840 nm and 960 nm normalized to the change found in the first spectrum acquired. Temperature at the radiance fibre is shown on the right axis. Results from experiment #1 using heating protocol ii).

4.3 Theoretical Radiance Results

Theoretical radiance calculations for the three different cases as described in section 3.4 are presented in figure 4.3.1. The features in case #1 are similar to the temperature-dependent changes of water absorption due to a 15°C temperature increase. In addition, changes in amplitude found in the experimental *ex vivo* tissue results (figure 4.2.4) match case #1 closest. Other cases do not match the experimental results very well as case #2 and #3 lack the spectral features found in the temperature-dependence of water absorption. Also, a 10% change in water content or scattering would have a much greater effect on the radiance measurements. A residual sum of squared errors between the experiment #2, protocol i), and the theoretical results was computed to compare the processed spectra. Experiment #2 protocol i) was chosen for comparison because the temperature difference between the spectra acquired in heated tissue and cooled tissue at the radiance detector was exactly 15°C the same as in the theoretical radiance calculations. Also, experiment #3 protocol i) was chosen for comparison because the spectra acquired between the first and last spectrum had undergone 13.8°C, which is close to theoretical

radiance calculations. Table 4.3.1 shows the residual sum of squares was least in case #1 where only temperature-dependent changes due to water affect the optical properties. The theoretical radiance calculations show that the changes in *ex vivo* tissue are due to temperature-dependent changes in water absorption.

Table 4.3.1: Residual sum of squares between the experiments 1 and 2 using heating protocol i) and the three cases using theoretical radiance calculations for wavelengths of 700 – 1000 nm.

Residual Sum of Squares	Case #1	Case #2	Case #3
Experiment #1	0.0044	15.3399	109.2013
Experiment #2	0.0054	14.9385	107.9708

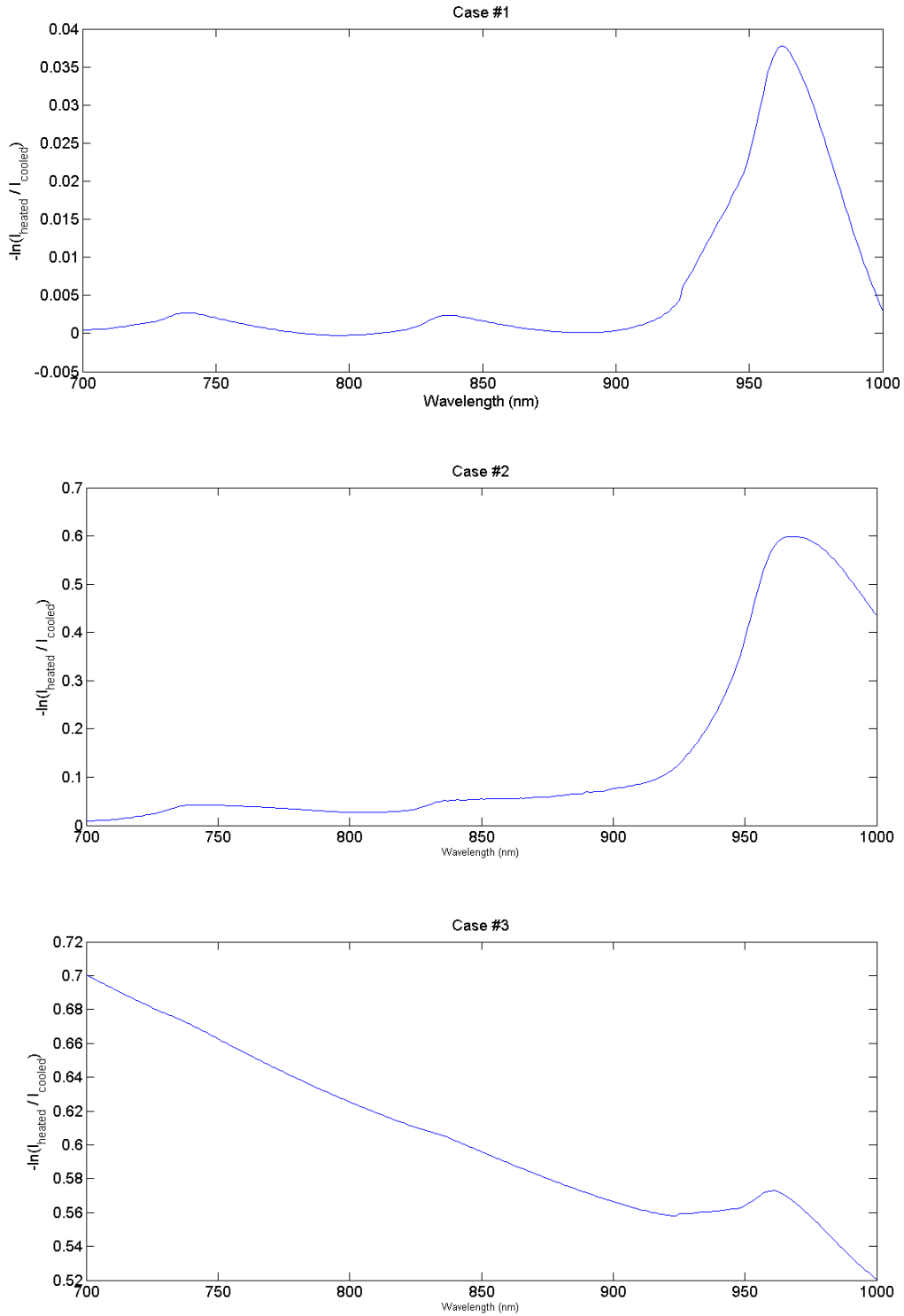


Figure 4.3.1: Theoretical radiance comparison between simulated heated tissue and cooled tissue. Case #1 represents changes due to temperature-dependent water absorption. Case #2 represents temperature-dependent water absorption and a 10% increase in water content. And case #3 represents temperature-dependent water absorption and 10% change in reduced scattering.

5 Conclusion and Future Work

5.1 Conclusions

The results demonstrate that the radiance signal mostly represents thermal damage but a small part of the signal represents a temperature-dependent change due to optical absorption of water.

This work has shown the radiance system is able to detect both the optical absorption and the temperature-dependent changes in the optical absorption of pure water. Although the exact absorption spectra cannot be measured the overall shape of the spectrum is detectable by comparing the spectra in air and water. Small temperature-dependent optical changes in water were detected by comparing heated water with room temperature water. The location in the spectrum where radiance measurements detected the temperature-dependent features of water at 739 nm, 837 nm and 962 nm agree with other investigators (Hollis, 2002, Langford *et al*, 2001). In addition, the collection angle of the radiance system in water changes in heated water. However, these changes are small and to relate these changes in acceptance angle in a turbid medium is difficult.

In the *ex vivo* porcine muscle experiments, the radiance signal during laser tissue heating undergoes a dynamic change. More specifically the optical signal gradually increases and the detected radiance signal in coagulated tissue was found to be higher than in native tissue. This differed from previous studies (Chin *et al*, 2004) using radiance to monitor tissue coagulation. The exact reason for this is outside the scope of this project but possible explanations can be due to using different tissue phantoms and heating protocol. The optical signal during the cooling of the coagulated tissue revealed that the dynamic changes in radiance mainly represent a permanent change. However, small temperature-dependent changes exist due to water based on the detected absorption peaks. Theoretical radiance calculations were performed to help explain possible differences between the spectra acquired in heated tissue and cooled tissue. The simulations indicate that temperature-dependent change in water best describes the amplitude of the detected changes and peaks at approximate wavelengths of 739 nm, 837 nm and 962 nm.

This work shows that radiance measurements using a cleaved fibre is a viable method to detect permanent change due to thermal damage during the monitoring of LITT.

5.2 Future Work

Fibres with a reflective coating on the hypotenuse should be used in the future. This would increase the fibre collection efficiency. The reflective coating would also eliminate, if not reduce, the amount of light entering the fibre from the opposite direction.

This study had observed different changes in the radiance signal than previous studies (Chin *et al*, 2004). It was hypothesized that the reason for these changes is due to low optical absorption causing slow heating time and resulting in the coagulation to be diffuse. An experiment to determine if this was the case can be conducted in tissue mimicking phantoms. Radiance measurements should be acquired during laser heating experiments in phantoms with low absorption and high absorption to determine the cause for the different optical signal.

Future work should include monitoring laser thermal therapy using radiance measurements in an *in vivo* study. This work has shown that the radiance signal represents mainly thermal damage and only a small fraction of the signal represents a reversible change due to heated water. In an *in vivo* study, the absorption coefficient will be higher due to higher blood content and will result in quicker heating times but this may also increase the risk of charring. However, heating may be reduced depending on the blood perfusion in the target. In addition, the signal in an *in vivo* study would be much lower due to higher optical absorption. This can introduce a low signal-to-noise ratio. *In vivo* studies on canine prostate should be conducted as this is the animal model chosen for validating new treatments for prostate (Schwartz *et al* 2011).

Future work can include investigating changes in water content due to thermal therapy as a diagnostic tool for thermal damage. During thermal therapy there is generally a loss in water content due to heat. The idea behind this approach is to measure the water content before heating and after heating. This can be done by measuring the spectral optical properties using a technique originally developed by Chin *et al* (2007). Fitting the major chromophore's of tissue to the spectral optical absorption can yield concentration of each chromophore, including water.

Radiance measurements as a diagnostic tool to determine the boundary of thermal damage should be investigated. Studies have investigated the use of radiance measurements to locate the

direction of inhomogeneities in tissue using an absorbing tube and 360° radiance data (Grabtchak *et al*, 2011). Similar studies can be undertaken to investigate if information can be recovered regarding the volumetric boundary of tissue coagulation based on changes in optical scattering using 360° radiance data.

Appendix

A Additional Measurements in Ex Vivo Tissue

Additional experiments in *ex vivo* tissue were performed but do not fall under the main experimental protocols. The information presented for these experiments will be: temperature-measurements during heating, normalized radiance during heating, ratio comparison between the first and the last acquired spectrum, and spectral changes during cooling. These experiments were not conducted with a particular heating time or maximum temperature.

Two experiments were conducted to determine if a decrease in the radiance signal can be observed far from the source. The experimental protocol differed from section 3.2 by placing the radiance fibre with the thermocouple 1 cm away from the detector instead of 0.5 cm. The coagulated region did not pass the radiance fiber, the border of the coagulated region stopped at the detector. Figures A.1 and A.2 show a different radiance signal change during heating. In one experiment the signal increased by ~20% and stayed relatively constant while in the other experiment the signal had decreased by 20%. Both experiments show spectral features of temperature-dependent water absorption at approximately 740 nm, 840nm and 960 nm. The experiment in figure A.1 shows an additional feature at ~775 nm. The ratio at ~960 nm appears to have much larger noise most likely due to a poor signal and detector response.

Experiments without a cooling catheter were conducted to determine if the cooling affects the heating time. The two experiments in figures A.3 and A.4 use a power of 6 watts and 8 watts, respectively. Lower powers were chosen to reduce the risk of charring the tissue since there is no water flow to reduce the heat at the cylindrical fiber. As a result maximum temperature would be at the center of the cylindrical diffuser. Using a power of 6 watts the coagulated tissue boundary reached the radiance detector. Using a power of 8 watts the radiance fiber was misaligned such that it was not positioned at the center of the diffuser more along the tip of the fiber. Again, the radiance signal had undergone different changes in the two experiments; the radiance signal increased in the experiment using 8 watts while a small decrease was observed using 6 watts of laser power. An interesting remark regarding the two experiments is that the temperature-dependent features are not well observable. Using 8 watts the temperature-dependent features are

detectable but are not the dominant feature as the 740 and 840 peaks vary in amplitude. Using a 6 watt laser power the ratio between the first and last spectrum resembles water absorption more than the temperature-dependent water absorption. However, not enough experiments were conducted to conclude if the water in the cooling catheter affects the optical signal.

The Diomed-15 laser from Princess Margaret Hospital was used to investigate if the long heating time was due to a problem with the laser used throughout the project. The Diomed-15 laser outputs a maximum power of 15 watts while the Diomed-60 outputs a maximum a power of 60 watts. Experimental results show a slightly longer heating time with the diomed-15 laser (figure A.5). As a result, there was no reason to suspect anything wrong with the Diomed-60 laser

In figure A.6, increasing laser power to 12 watts does increase the rate at which high temperatures are achieved but not significantly, in other words the time to reach 55°C at the radiance fiber is still over 25 minutes. The last experiment shown in figure A.7 is similar to the experiments conducted in the section 3 but does not fall under any of the main protocols.

Although different heating protocols have been used, the rate of heating typically exceeded 25 minutes. Overall all experiments, except for one, show the spectral features of temperature-depedent changes in water absorption at approximately 740 nm, 840 nm and 960 nm.

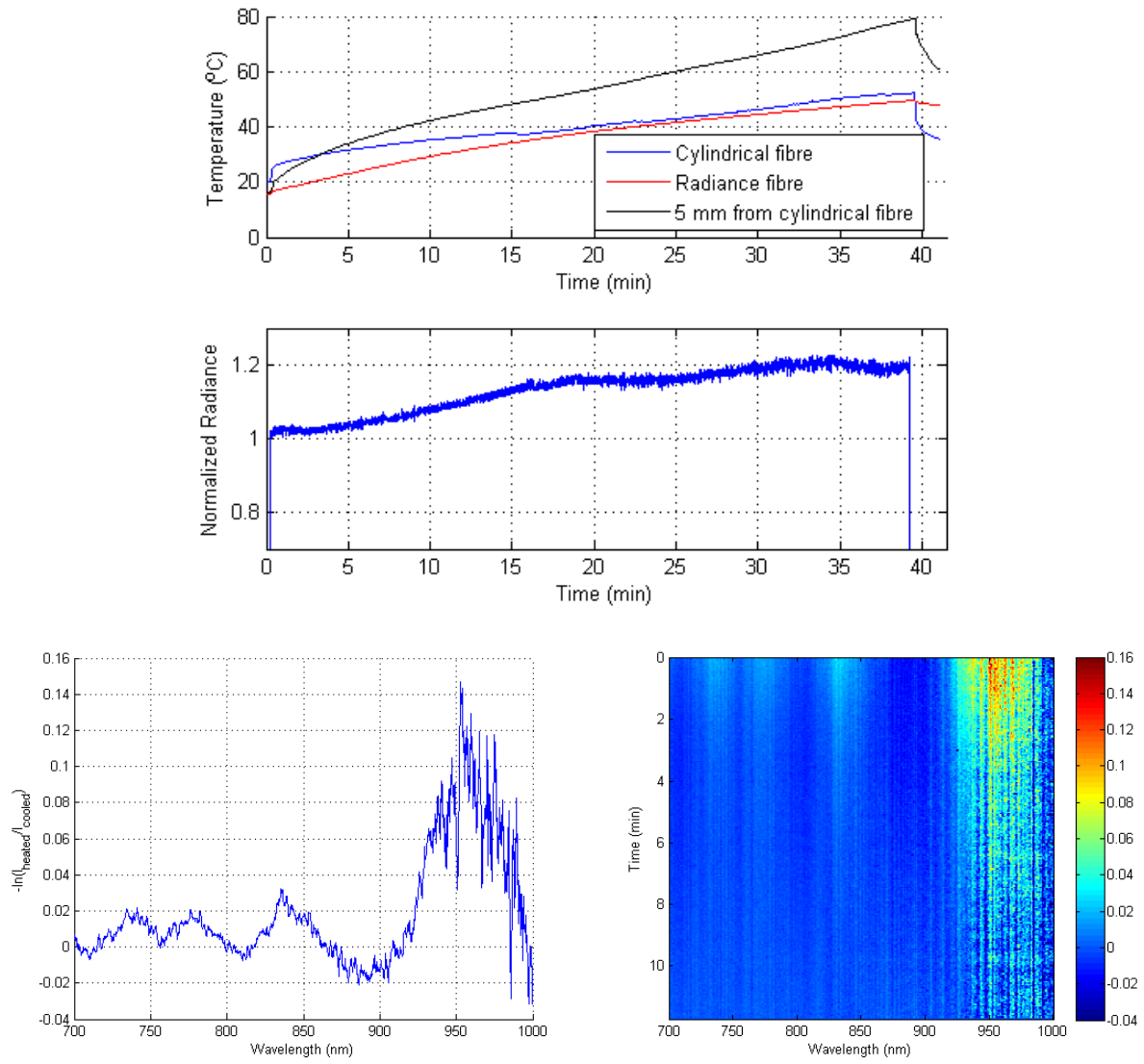


Figure A.1: Tissue heating experiment using 10 watt laser power. Source-detector distance 1 cm.

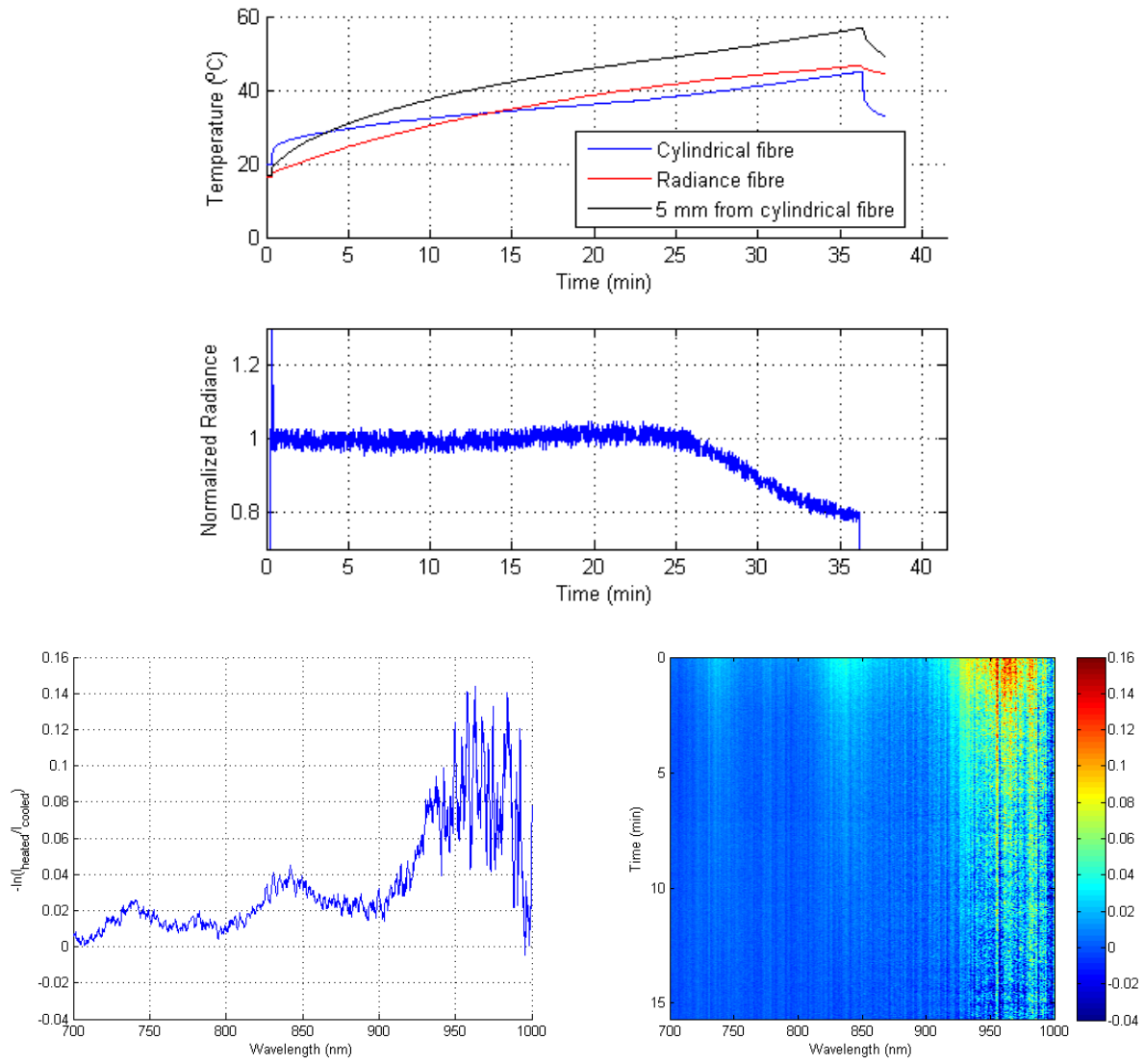


Figure A.2: Tissue heating experiment using 10 watt laser power. Source-detector distance 1 cm.

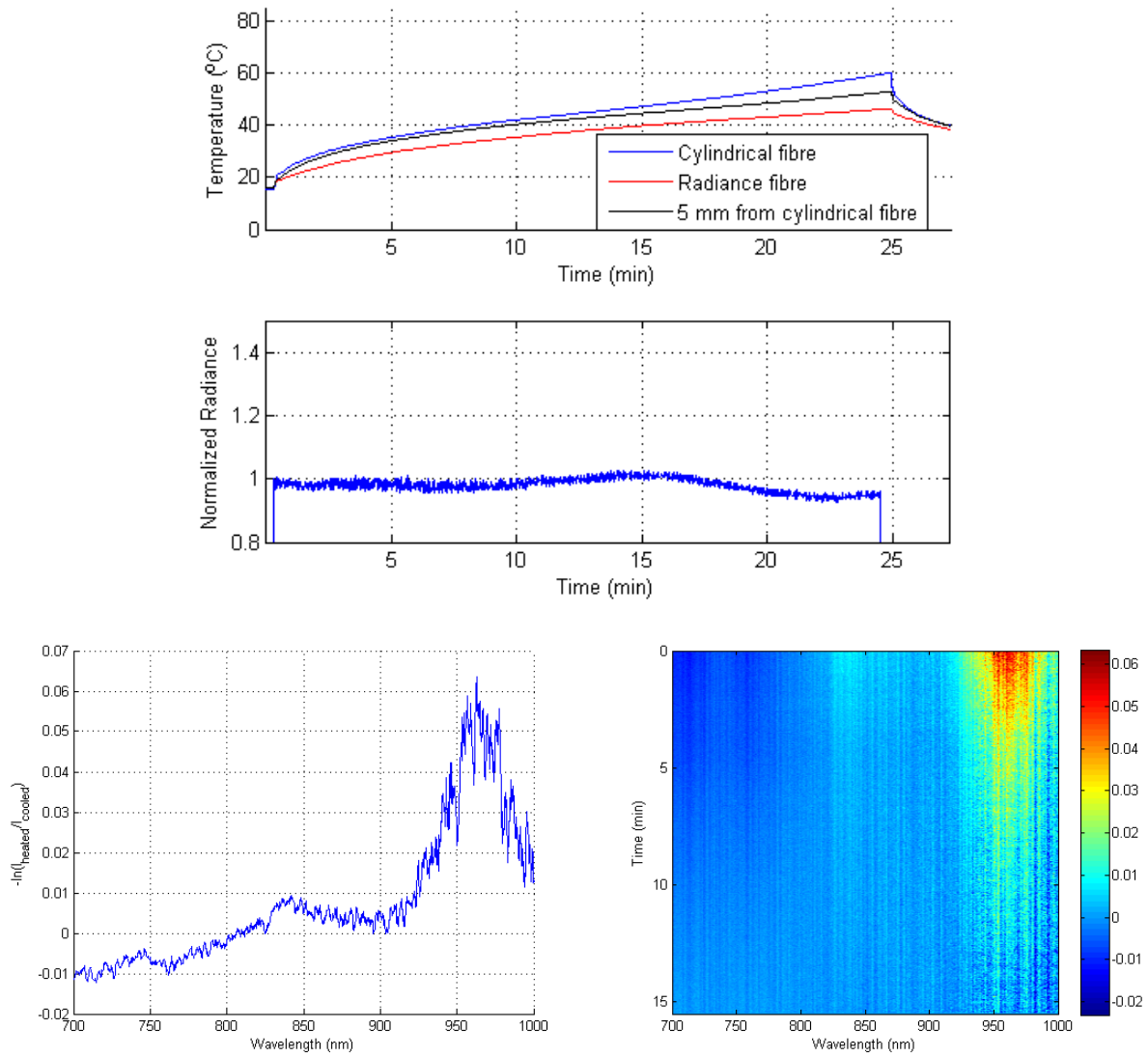


Figure A.3: Tissue heating experiment using 6 watts laser power with no cooling catheter. Source-detector distance of 5 mm.

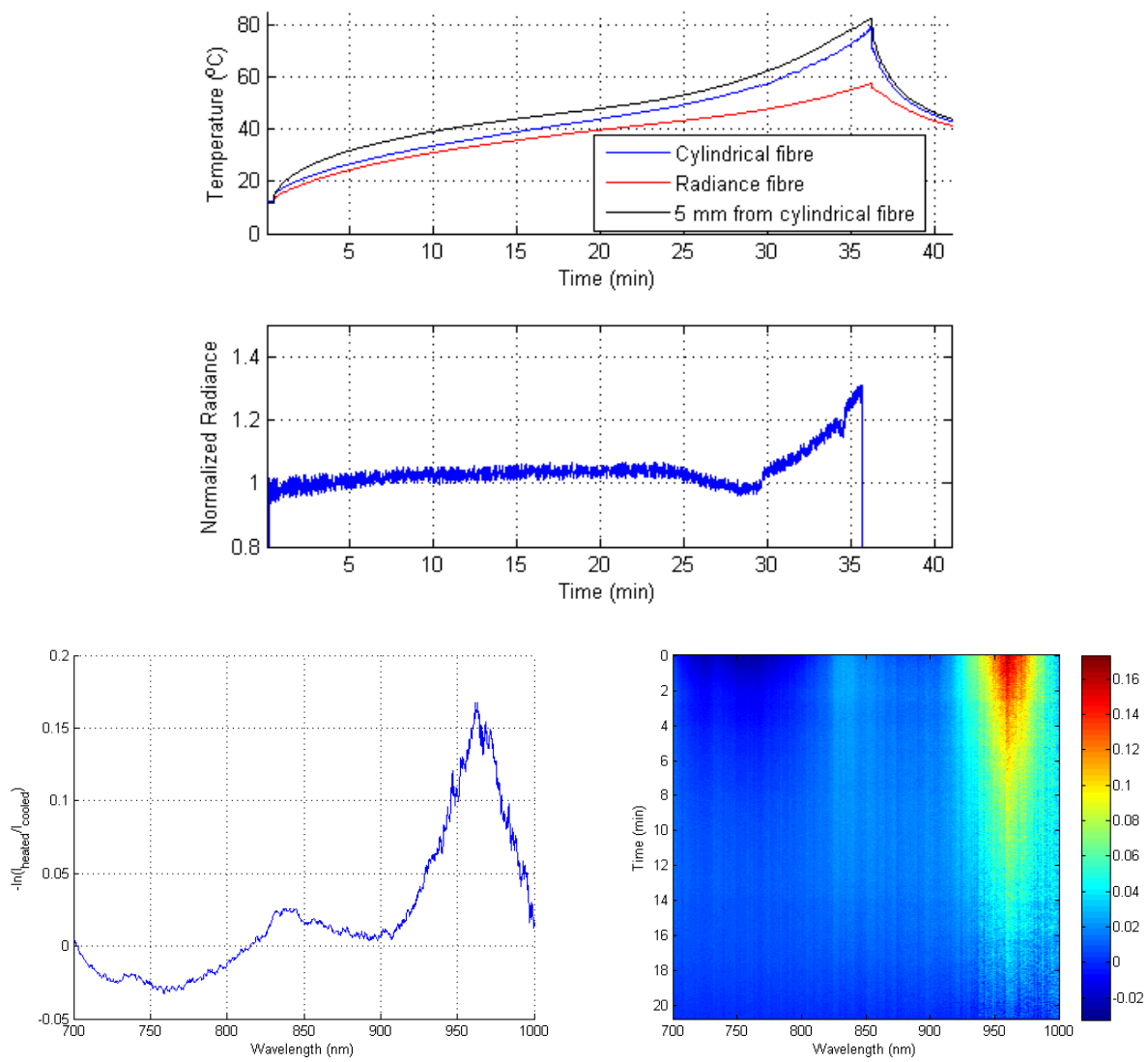


Figure A.4: Tissue heating using 8 watts laser power. No cooling catheter. Source detector distance of 5 mm.

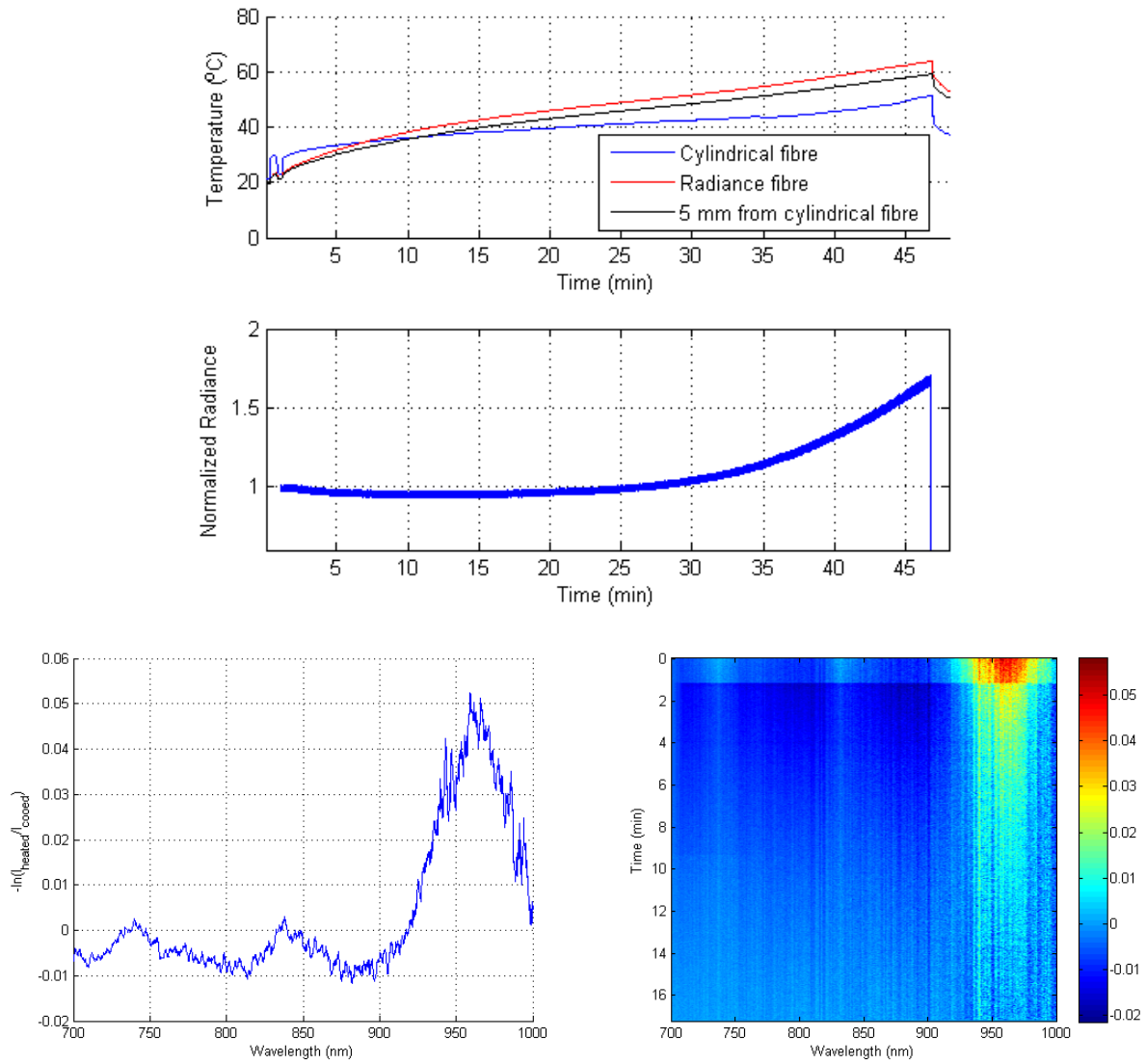


Figure A.5: Tissue heating experiment using 10 watts laser power with the diomed-15 laser. Source detector distance of 5 mm.

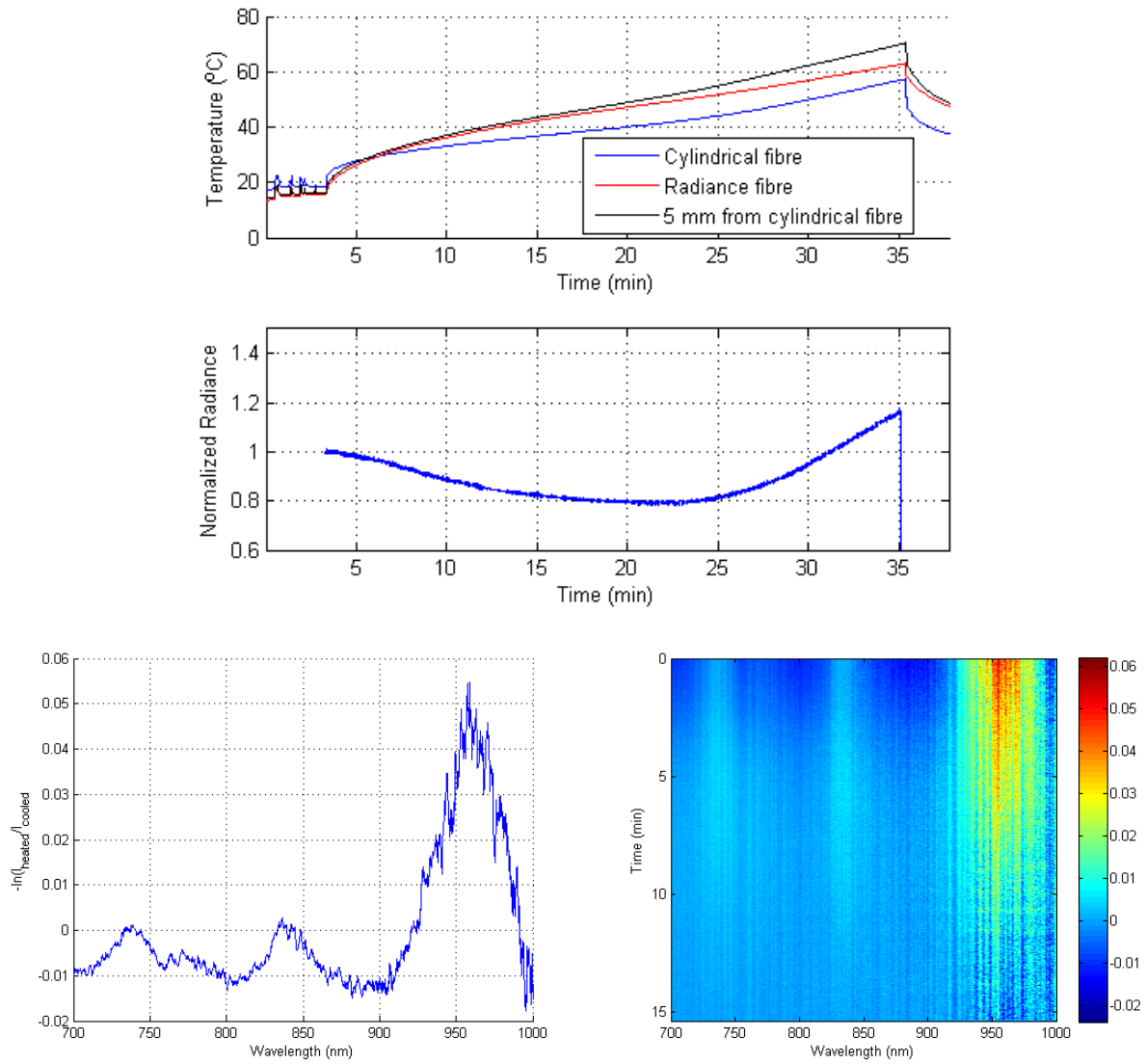


Figure A.6: Tissue heating experiment using 12 watts laser power. Source detector distance of 5 mm.

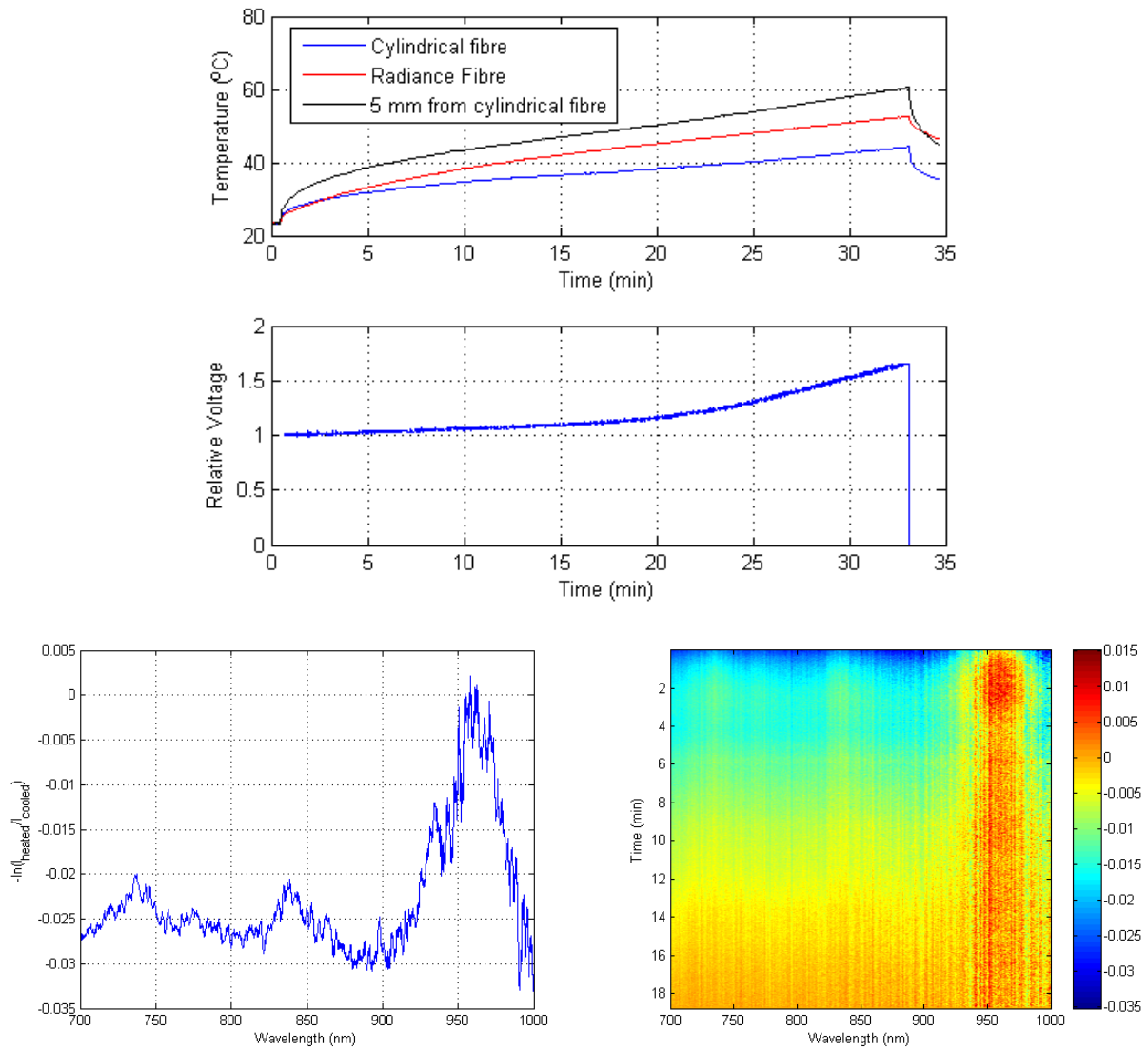


Figure A.7: Tissue heating experiment using 10 watts laser power. Source-detector distance of 5 mm.

B Diffuse Reflectance Measurements

Diffuse reflectance data was acquired in an attempt to recover the optical properties of both the native tissue and coagulated tissue. The diffuse reflectance set-up was created by Dr. Anthony Kim. The set-up consists of a light source connected to a fibreoptic bundle with a SMA 905 connector. The fibreoptic bundle has multiple fibers spaced at various distance in a line. The distances from the light emitting fibre are: 0.8, 1.5, 2.4, 4.0, 5.3 mm. These fibres are connected to a multiplexor. The multiplexor is then connected to a spectrometer using another optical fibre. The system works by collecting light from each fiber consecutively. The system is a *one light source with multiple detector* set-up. An integration time of 10 seconds was used with a boxcar filter of 4.

Two different samples of 3% of Intralipid 20% was used for calibration at 800 nm. Diffuse reflectance measurements of the first Intralipid sample was measured ~ 20 days before performing diffuse reflectance measurements on native porcine muscle. The fibreoptic probe was hand-held during acquisition. While the diffuse reflectance measurements of Intralipid for coagulated tissue were taken the same day. For measurements on coagulated tissue, the fibreoptic probe was held using a clamp.

Theoretical diffuse reflectance is based on Farrell *et al* (1992) given by the following equation:

$$R_{DT}(\lambda, r) = \frac{a'}{4\pi} \left[z_o \left(1 + \frac{1}{r_1} \right) \frac{e^{-\mu_{eff} r_1}}{r_1^2} + (z_o + 2z_b) \left(1 + \frac{1}{r_2} \right) \frac{e^{-\mu_{eff} r_2}}{r_2^2} \right], \quad (6.1)$$

where $a' = \mu_s' / (\mu_a + \mu_s')$, $z_o = 1/\mu_s'$, $r_1^2 = z_o^2 + r^2$, $r_2^2 = (z_o + 2z_b)^2 + r^2$, $z_b = 2\kappa D$, $\kappa = (1 + r_{id}) / (1 - r_{id})$, $r_{id} = -1.44n_{rel}^{-2} + 0.71n_{rel}^{-1} + 0.67 + 0.0636n_{rel}$, $n_{rel} = 1.4/1$, $D = (3\mu_s')$ and $\mu_{eff} = (3\mu_a\mu_s')^{1/2}$. Where μ_a and μ_s' are wavelength dependent and r is the source-detector distance

All diffuse reflectance measurements and calculations were normalized to the first source-detector distance. The system was calibrated using the following equations:

$$Scale(\lambda, r) = \frac{R_{DT}}{R_{measured}}, \quad (6.2)$$

where $R_{measured}$ and R_{DT} are the measured diffuse reflectance in Intralipid and theoretical diffuse reflectance signals respectively. Absorption of zero and a reduced scattering of 5.09 cm^{-1} were

used to generate the theoretical diffuse reflectance values at 800 nm. The calibrated data was found using the following:

$$\text{calibrated data} = \text{Scale} \times R_{\text{tissue}}, \quad (6.3)$$

where R_{tissue} is the measured data in *ex vivo* porcine tissue. The calibrated tissue data is simply the Scale multiplied by the measured diffuse reflectance for each source-detector. The calibrated data was then optimized to find the best solution to equation 6.1 using Matlab's *fminsearch* algorithm. The program was limited to recover only positive values for μ_a and μ_s .

The data for native porcine tissue do not fit well as illustrated in figure A.1 but were consistent for three trials. The recovered μ_a were very close to zero suggesting the optical absorption may have been very low and outside the detectability of the diffuse reflectance system. The data in coagulated tissue had a much better fit as shown in figure A.2. However, the recovered absorption coefficient was $\sim 1 \text{ cm}^{-1}$, which is very high. Such a value is expected in liver where large amounts of blood is present causing a high absorption and was not expected in the porcine muscle used. Possible discrepancy can be due to the calibration process. If using the scaling factors found in the first Intralipid sample instead the recovered absorption coefficient is approximately 40% less. This suggests a change in the actual optical properties of the Intralipid sample with time.

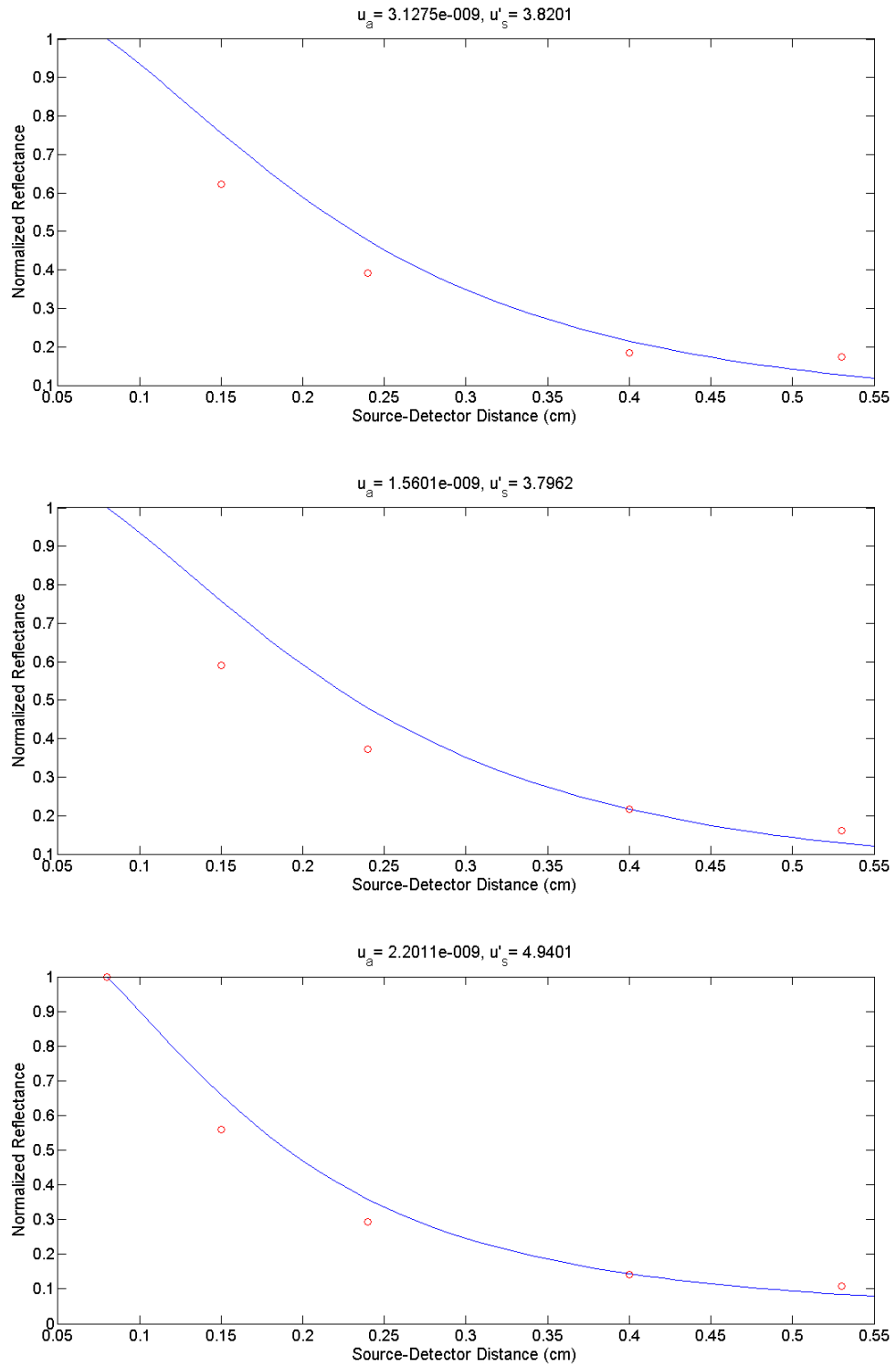


Figure B.1: Three trials of diffuse reflectance data in native porcine muscle. Theoretical diffuse reflectance in blue fitted to the measured diffuse reflectance in red.

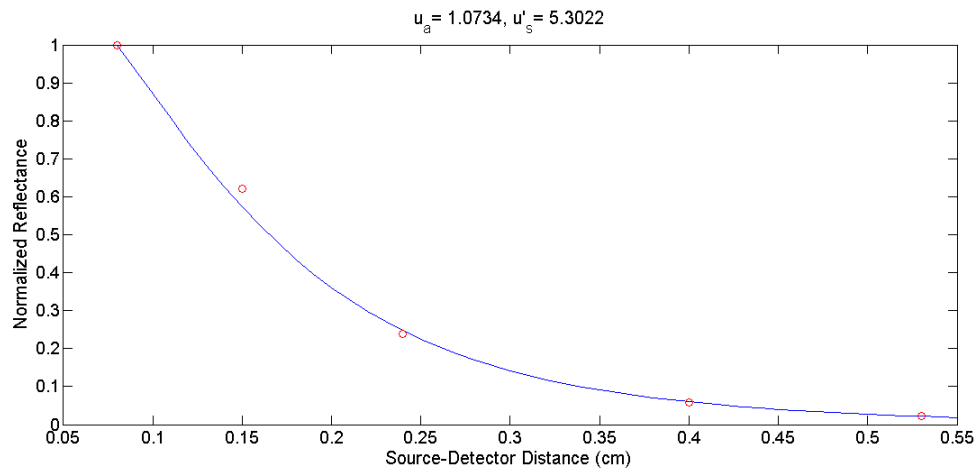
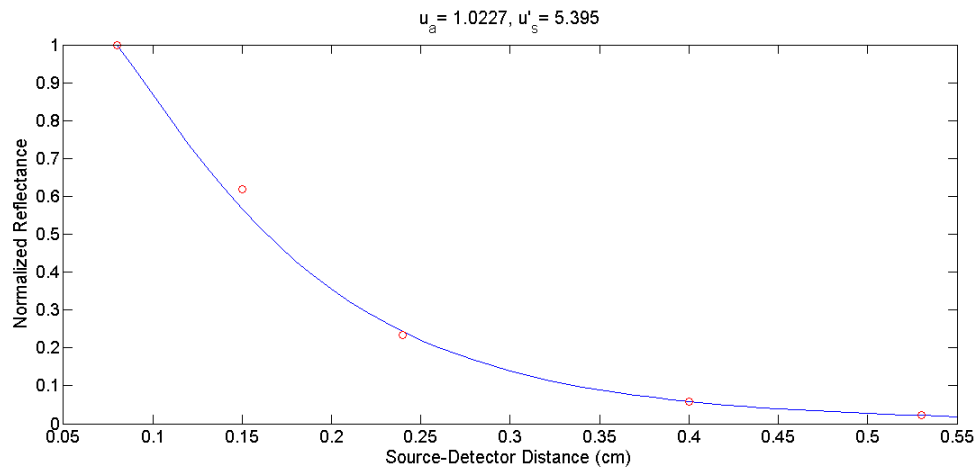
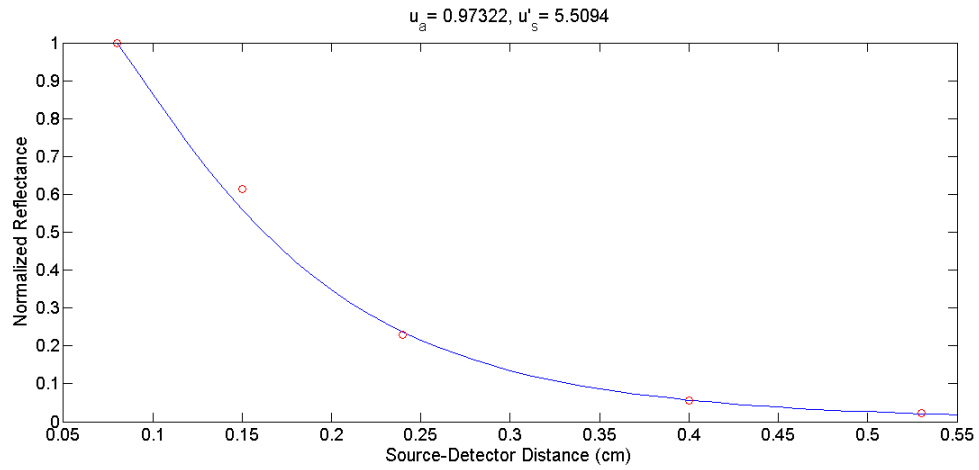


Figure B.2: Three trials of diffuse reflectance data in coagulated porcine muscle. Theoretical reflectance in blue fitted to the measured reflectance in red.

Bibliography

(2011) *Canadian Cancer Statistics 2011*. Canadian Cancer Society's Steering Committee. Toronto: Canadian Cancer Society

Arsenault, M. G., Kolios, M. C., & Whelan, W. M. (2009). Optoacoustic detection of thermal lesions. Paper presented at the *Progress in Biomedical Optics and Imaging - Proceedings of SPIE*, 7177

Ben-Eliyahu, S. (2002). The price of anticancer intervention. does surgery promote metastasis? *The Lancet Oncology*, 3(9), 578-579

Bown, S.G. (1983). Phototherapy of tumors. *World Journal of Surgery*, 7 (6), 700-709

Carpentier, A., McNichols, R. J., Stafford, R. J., Itzcovitz, J., Guichard, J., Reizine, D., Delalogue, S., Vicaut, E., Payen, D., Gowda, A., George, B. (2008). Real-time magnetic resonance-guided laser thermal therapy for focal metastatic brain tumors. *Neurosurgery*, 63(1 SUPPL.), ONS21-ONS28

Cheong, W.F. 1995. *Summary of optical properties*. Optical-Thermal Response of Laser-Irradiated Tissue, New York: Plenum Press (Appendix to Chapter 8)

Chin, L. C. L., Worthington, A. E., Whelan, W. M., & Vitkin, I. A. (2007). Determination of the optical properties of turbid media using relative interstitial radiance measurements: Monte carlo study, experimental validation, and sensitivity analysis. *Journal of Biomedical Optics*, 12(6)

Chin, L. C. L., Whelan, W. M., & Vitkin, I. A. (2007). Perturbative diffusion theory formalism for interpreting temporal light intensity changes during laser interstitial thermal therapy. *Physics in Medicine and Biology*, 52(6), 1659-1674

Chin, L. C. L., Wilson, B. C., Whelan, W. M., & Vitkin, I. A. (2004). Radiance-based monitoring of the extent of tissue coagulation during laser interstitial thermal therapy. *Optics Letters*, 29(9), 959-961.

Chitnis, P. V., Brecht, H., Su, R., & Oraevsky, A. A. (2010). Optoacoustic imaging of HIFU-induced thermal lesions in tissue. Paper presented at the *Progress in Biomedical Optics and Imaging - Proceedings of SPIE*, 7564

Chung, S.H., Cerussi, A.E., Merritt, S.I., Ruth, J., Tromberg, B.J. (2010). Non-invasive tissue temperature measurements based on quantitative diffuse optical spectroscopy (DOS) of water. *Physics in Medicine and Biology*, 55(13), 3753-3765

Collins, J.R. (1925). Change in the infra-red absorption spectrum of water with temperature. *Physical Review*, 26 (6), 771-779

Cletus, B., Künnemeyer, R., Martinsen, P., & McGlone, V. A. (2010). Temperature-dependent optical properties of intralipid measured with frequency-domain photon-migration spectroscopy. *Journal of Biomedical Optics*, 15(1), 017003

Daimon, M., & Masumura, A. (2007). Measurement of the refractive index of distilled water from the near-infrared region to the ultraviolet region. *Applied Optics*, 46(18), 3811-3820

Davidson, S. R. H., Vitkin, I. A., Sherar, M. D., & Whelan, W. M. (2005). Characterization of measurement artefacts in fluoroptic temperature sensors: Implications for laser thermal therapy at 810 nm. *Lasers in Surgery and Medicine*, 36(4), 297-306

Farrell, T. J., Patterson, M. S., & Wilson, B. (1992). A diffusion theory model of spatially resolved, steady-state diffuse reflectance for the noninvasive determination of tissue optical properties in vivo. *Medical Physics*, 19(4), 879-888

Garcia-Medina, O., Gorny, K., McNichols, R., Friese, J., Misra, S., Amrami, K., et al. (2011). In vivo evaluation of a MR-guided 980nm laser interstitial thermal therapy system for ablations in porcine liver. *Lasers in Surgery and Medicine*, 43(4), 298-305

Gertner, M. R., Wilson, B. C., & Sherar, M. D. (1997). Ultrasound properties of liver tissue during heating. *Ultrasound in Medicine and Biology*, 23(9), 1395-1403

Grabtchak, S., Palmer, T. J., & Whelan, W. M. (2011). Detection of localized inclusions of gold nanoparticles in intralipid-1% by point-radiance spectroscopy. *Journal of Biomedical Optics*, 16(7)

Henriques Jr., F.C. (1947). Studies of thermal injury. V. The predictability and the significance of thermally induced rate process leading to irreversible epidermal injury. *Archives of Pathology*, 43, 489-502

Van Hillegersberg, R., Van Staveren, H. J., Kort, W. J., Zondervan, P. E., & Terpstra, O. T. (1994). Interstitial Nd:YAG laser coagulation with a cylindrical diffusing fiber tip in experimental liver metastases. *Lasers in Surgery and Medicine*, 14(2), 124-138

Hollis, V. (2002). Non-invasive monitoring of brain tissue temperature by near-infrared spectroscopy. PhD Thesis University College London

Inoue, Y., Goto, K., Hayashi, T., & Hayashi, M. (2011). Transrectal high-intensity focused ultrasound for treatment of localized prostate cancer. *International Journal of Urology*, 18(5), 358-363

Jacques, S.L., Prahl, S.A. (1998), <http://omlc.ogi.edu/classroom/ece532/>

Kienle, A., Lilge, L., Patterson, M. S., Hibst, R., Steiner, R., & Wilson, B. C. (1996). Spatially resolved absolute diffuse reflectance measurements for noninvasive determination of the optical scattering and absorption coefficients of biological tissue. *Applied Optics*, 35(13), 2304-2314

- Konishi, K., Maehara, T., Kamimori, T., Aono, H., Naohara, T., Kikkawa, H., et al. (2004). Heating ferrite powder with AC magnetic field for thermal coagulation therapy. *Journal of Magnetism and Magnetic Materials*, 272-276(III), 2428-2429
- Liemert, A., Kienle, A., (2011). Analytical green's function of the radiative transfer radiance for the infinite medium. *Physical Review*, 83(3), 036605
- Langford, V. S., McKinley, A. J., & Quickenden, T. I. (2001). Temperature dependence of the visible-near-infrared absorption spectrum of liquid water. *Journal of Physical Chemistry A*, 105(39), 8916-8921
- Larin, K. V., Larina, I. V., & Esenaliev, R. O. (2005). Monitoring of tissue coagulation during thermotherapy using optoacoustic technique. *Journal of Physics D: Applied Physics*, 38(15), 2645-2653
- Matcher, S. J., Cope, M., & Delpy, D. T. (1994). Use of the water absorption spectrum to quantify tissue chromophore concentration changes in near-infrared spectroscopy. *Physics in Medicine and Biology*, 39(1), 177-196
- McGlone, V. A., Martinsen, P., Künnemeyer, R., Jordan, B., & Cletus, B. (2007). Measuring optical temperature coefficients of intralipid®. *Physics in Medicine and Biology*, 52(9), 2367-2378
- McNichols, R. J., Gowda, A., Kangasniemi, M., Bankson, J. A., Price, R. E., & Hazle, J. D. (2004). MR thermometry-based feedback control of laser interstitial thermal therapy at 980 nm. *Lasers in Surgery and Medicine*, 34(1), 48-55
- Mourant, J. R., Fuselier, T., Boyer, J., Johnson, T. M., & Bigio, I. J. (1997). Predictions and measurements of scattering and absorption over broad wavelength ranges in tissue phantoms. *Applied Optics*, 36(4), 949-957
- Pearce J, Thomsen S. *Rate process analysis of thermal damage*. Optical-Thermal Response of laser-Irradiated Tissue. New York: Plenum Press, 1995
- Potosky, A. L., Davis, W. W., Hoffman, R. M., Stanford, J. L., Stephenson, R. A., Penson, D. F., et al. (2004). Five-year outcomes after prostatectomy or radiotherapy for prostate cancer: The prostate cancer outcomes study. *Journal of the National Cancer Institute*, 96(18), 1358-1367
- Quesson, B., De Zwart, J. A., & Moonen, C. T. W. (2000). Magnetic resonance temperature imaging for guidance of thermotherapy. *Journal of Magnetic Resonance Imaging*, 12(4), 525-533
- Reid, A. D., Gertner, M. R., & Sherar, M. D. (2001). Temperature measurement artefacts of thermocouples and fluoroptic probes during laser irradiation at 810 nm. *Physics in Medicine and Biology*, 46(6), N149-N157

- Sapareto, S.A., Dewey, W.C. (1984). Thermal dose determination in cancer therapy *International Journal of Radiation Oncology Biology Physics*, 10(6), 787-800
- Schaeffer, E. M., Loeb, S., & Walsh, P. C. (2010). The case for open radical prostatectomy. *Urologic Clinics of North America*, 37(1), 49-55
- Schwartz, J. A., Price, R. E., Gill-Sharp, K. L., Sang, K. L., Khorchani, J., Goodwin, B. S., et al. (2011). Selective nanoparticle-directed ablation of the canine prostate. *Lasers in Surgery and Medicine*, 43(3), 213-220
- Shelley, M., Harrison, C., Coles, B., Staffurth, J., Wilt, T. J., & Mason, M. D. (2006). Chemotherapy for hormone-refractory prostate cancer. *Cochrane Database of Systematic Reviews*, (4)
- Sherar, M. D., Trachtenberg, J., Davidson, S. R. H., McCann, C., Yue, C. K. K., Haider, M. A., et al. (2003). Interstitial microwave thermal therapy for prostate cancer. *Journal of Endourology*, 17(8), 617-625
- Simpson, C. R., Kohl, M., Essenpreis, M., & Cope, M. (1998). Near-infrared optical properties of ex vivo human skin and subcutaneous tissues measured using the monte carlo inversion technique. *Physics in Medicine and Biology*, 43(9), 2465-2478
- Skinner, M. G., Everts, S., Reid, A. D., Vitkin, I. A., Lilge, L., & Sherar, M. D. (2000). Changes in optical properties of ex vivo rat prostate due to heating. *Physics in Medicine and Biology*, 45(5), 1375-1386
- Svensson, T., Andersson-Engels, S., Einarsdóttir, M., & Svanberg, K. (2007). In vivo optical characterization of human prostate tissue using near-infrared time-resolved spectroscopy. *Journal of Biomedical Optics*, 12(1)
- Sun, F., Wentong, Z., Yan, Z., Qingyu, D., & Aiwu, L. (2006). Application of endoscopic ho:YAG laser incision technique treating urethral strictures and urethral atresias in pediatric patients. *Pediatric Surgery International*, 22(6), 514-518
- Tracz, R. A., Wyman, D. R., Little, P. B., Towner, R. A., Stewart, W. A., Schatz, S. W., et al. (1993). Comparison of magnetic resonance images and the histopathological findings of lesions induced by interstitial laser photocoagulation in the brain. *Lasers in Surgery and Medicine*, 13(1), 45-54
- Toyoda, T., & Yabe, M. (1983). The temperature dependence of the refractive indices of fused silica and crystal quartz. *Journal of Physics D: Applied Physics*, 16(5), L97-L100
- Whelan, W. M., & Wyman, D. R. (1999). Dynamic modeling of interstitial laser photocoagulation: Implications for lesion formation in liver in vivo. *Lasers in Surgery and Medicine*, 24(3), 202-208

Wu, F., Wang, Z., Cao, Y., & Hazle, J. D. (2004). A randomised clinical trial of high-intensity focused ultrasound ablation for the treatment of patients with localised breast cancer. *Breast Diseases*, 15(3), 291